BIOENERGETIC CONSEQUENCES OF HETEROZYGOUS ALPHA-KETOGLUTARATE DEHYDROGENASE COMPLEX MUTATION

PhD thesis

Márton Kokas, M.D.

Semmelweis University Doctoral College

Szentágothai János Neurosciences Division

Supervisors: László Tretter, M.D., D.Sc.

Tímea Komlódi, Pharm. D., Ph.D.

Official reviewers: Balázs Radnai, Ph.D.

Csaba Konrád, Pharm.D., Ph.D.

Head of the Complex Examination Committee: Tamás Mészáros, D.Sc.

Members of the Complex Examination Committee: Enikő Hocsák, Ph.D.

Tamás Kardon, Ph.D.

Budapest

2026

Table of contents:

Abbreviations:

α-KG – α-ketoglutarate

$\Delta\Psi_m$ – mitochondrial membrane potential

ADP – adenosine diphosphate

Ama – antimycin A

AP5 – P1,P5-di(adenosine-5′)-pentaphosphate

ATP – adenosine triphosphate

BSA – bovine serum albumin

CAT – Carboxyatractyloside

CI, II, III, IV – mitochondrial complex I, II, III, IV

CoA – coenzyme A

DBS – dried blood spots

DKO – DLST and DLD double heterozygous knockout ($DLST^{+/-}$-$DLD^{+/-}$)

DLD, E3 – dihydrolipoyl dehydrogenase

DLST, E2k – dihydrolipoyl succinyltransferase

(d)NTP – (deoxy)nucleotide triphosphate

Drp1 – dynamin-related protein 1

E/e' – Early mitral valve peak blood-flow velocity/ early mitral annulus peak movement velocity

EDV – end diastolic volume

EF – ejection fraction

EGTA – ethylene glycol-bis(β-aminoethyl ether)-N,N,N′,N′-tetraacetic acid

ESV – end systolic volume

ETS – electron transfer system

FA – fatty acid

$FAD/FADH_2$ – oxidised/reduced flavin adenine dinucleotide

FCCP – carbonyl cyanide-p-trifluoromethoxyphenylhydrazone

FDG – [^{18}F]-fluorodeoxyglucose

FS – fractional shortening

G6PDH – glucose-6-phosphate dehydrogenase

HK – hexokinase

HR – heart rate

HRP – horseradish peroxidase

IDH3 – mitochondrial NAD^+-dependent isocitrate dehydrogenase

IMS – inter membrane space

IR – ischaemia-reperfusion

IVRT – isovolumetric relaxation time

LA – lipoic acid

LV – left ventricular

LVAWs/d – end systolic/diastolic LV anterior wall thicknesses

LVEDV – left ventricular end-diastolic volume

LVESV – left ventricular end-systolic volume

LVIDs/d – end systolic/diastolic left ventricular diameter

LVPWs/d – end systolic/diastolic LV posterior wall thicknesses

LVRI – left ventricular remodelling index

KGDHc – alpha-ketoglutarate dehydrogenase complex

KGDH/OGDH, E1k – ketoglutarate dehydrogenase

MDH – malate dehydrogenase

Mfn2 – mitofusin 2

MTFA – mitochondrial transcription factor A

NAD(P)/NAD(P)H – oxidised/reduced nicotinamide adenine dinucleotide (phosphate)

Nrf2 – nuclear factor (erythroid-derived 2)-like 2

oligo – oligomycin

OXPHOS – oxidative phosphorylation

PCR – polymerase chain reaction

PDHc – pyruvate dehydrogenase complex

PGC-1α – peroxisome proliferator-activated receptor gamma coactivator 1-α

P_i – inorganic phosphate

PMSF – phenylmethyl sulfonyl fluoride

POS – polarographic oxygen sensor

PTP – permeability transition pore

Q/QH_2 – coenzyme Q (oxidised ubiquinone/reduced ubiquinol form)

RER – respiratory exchange ratio

RET – reverse electron transfer

ROS – reactive oxygen species

rot – rotenone

SDH – succinate dehydrogenase

SLP – substrate-level phosphorylation

Succ, S – succinate

SUV – standardized uptake value

SV – stroke volume

TCAc – tricarboxylic acid cycle

TPP – thiamine pyrophosphate

TUNEL – terminal deoxynucleotidyl transferase-mediated dUTP-biotin nick end labelling

WT – wild type, control

I. Introduction:

Basic knowledge of mitochondria

The evolution of eukaryotes was a fundamental step that allowed multiple specialized cell types to function together in a complex organism. The compartmentalisation of eukaryotic cells is a crucial advantage compared with prokaryotes, allowing cellular processes to be precisely regulated under different conditions provided by the environment. Lane even states that without this symbiosis, life could not have evolved into the form with which we are familiar (1). One of the ubiquitous organelles inside the animal cells is the mitochondrion, which used to be a motile prokaryotic parasite that was incorporated by an archaic amoeba (2).

Mitochondria were first discovered in the 1840s (3). Later, in 1890, Richard Altman described mitochondria as “elementary organisms” inside the cells and called them “bioblasts” (4). The name ‘mitochondrion’ was given by Carl Benda who used the Greek *mito* (thread) and *chondros* (granule) words (5). In the first half of the 20th century many scientists (including the Nobelist Otto von Warburg) suggested that mitochondria play a crucial part in redox homeostasis and in the reduction of oxygen to water (for review see (3)). Nevertheless, the central role of mitochondria in cellular respiration was proved only in the middle of the century by Lazarow and Cooperstein (6). Mitochondria have their own bacteria-like circular DNAs, but most of their proteins are encoded on nuclear DNA (7).

Mitochondria are often referred to as the "powerhouses of the cell," and while this is true, they are far more multifaceted than a simple energy-producing factory. They have a vital role in intracellular calcium homeostasis (8-12), in apoptosis (13, 14), and in reactive oxygen species (ROS) balance (production and elimination) (15-17). ROS may not be the best term, since H_2O_2 molecule is one of the most important members of this group, even though it has no unpaired electron and not a free radical. Furthermore, the above-mentioned aspects regulate the opening of the permeability transition pore (PTP), which is a key factor for intrinsic apoptosis (14, 18, 19).

Mitochondria are surrounded by a double membrane, called the outer and inner membrane. These membranes separate the inter membrane space (IMS) (between the two membranes) and the mitochondrial matrix (located inside the inner membrane) from the

cytosol of the cell. The matrix is slightly more basic (pH ~ 8) compared to the IMS, which is caused by the proton pumps (associated with Complexes I, III and IV) of the electron transfer system (ETS, also known as electron transport chain) (20). The electron flow converges from CI; CII; α-glycerophosphate dehydrogenase or electron-transferring flavoprotein to Coenzyme Q, from where electrons enter the Q-cycle within CIII. The water-soluble cytochrome *c* molecule transfers the electrons to CIV, where the final electron acceptor, molecular oxygen, is reduced to H_2O. This difference in proton concentration between the matrix and the IMS leads to the electrochemical gradient that is the driving force for adenosine triphosphate (ATP) synthesis from adenosine diphosphate (ADP) and inorganic phosphate (P_i) (21, 22). This process is called oxidative phosphorylation (OXPHOS) because oxygen is required as the final electron acceptor to maintain electron flow via the ETS, and thus the proton pump activity of the complexes.

To maintain the proton gradient, mitochondria need reducing equivalents, namely nicotinamide adenine dinucleotide (NAD^+, reduced form is $NADH+H^+$) and flavin adenine dinucleotide (FAD, reduced form is $FADH_2$) (Fig. 1). The most common source of reducing equivalents is the tricarboxylic acid cycle (TCAc), which provides 3 $NADH+H^+$ (by the following enzymes: NAD^+-dependent isocitrate dehydrogenase, IDH3; alpha-ketoglutarate dehydrogenase complex, KGDHc; malate dehydrogenase; MDH) and 1 $FADH_2$ (succinate dehydrogenase; SDH) during one turn of the cycle. Additionally, from every glucose molecule two pyruvate molecules are produced which can be converted via oxidative decarboxylation into acetyl-CoA, meanwhile NAD^+ is reduced by the pyruvate dehydrogenase complex (PDHc). Furthermore, activated fatty acids (FA) produce NADH and $FADH_2$ in the ß-oxidation and ketone bodies or amino acids (namely lysine, leucine, isoleucine, tryptophan, tyrosine, phenylalanine) can also supply the mitochondria with acetyl-CoA. Of note, the TCAc has many anaplerotic reactions, which can supply the cycle with additional carbon skeletons, thus enhancing the production of reducing equivalents (23-25).

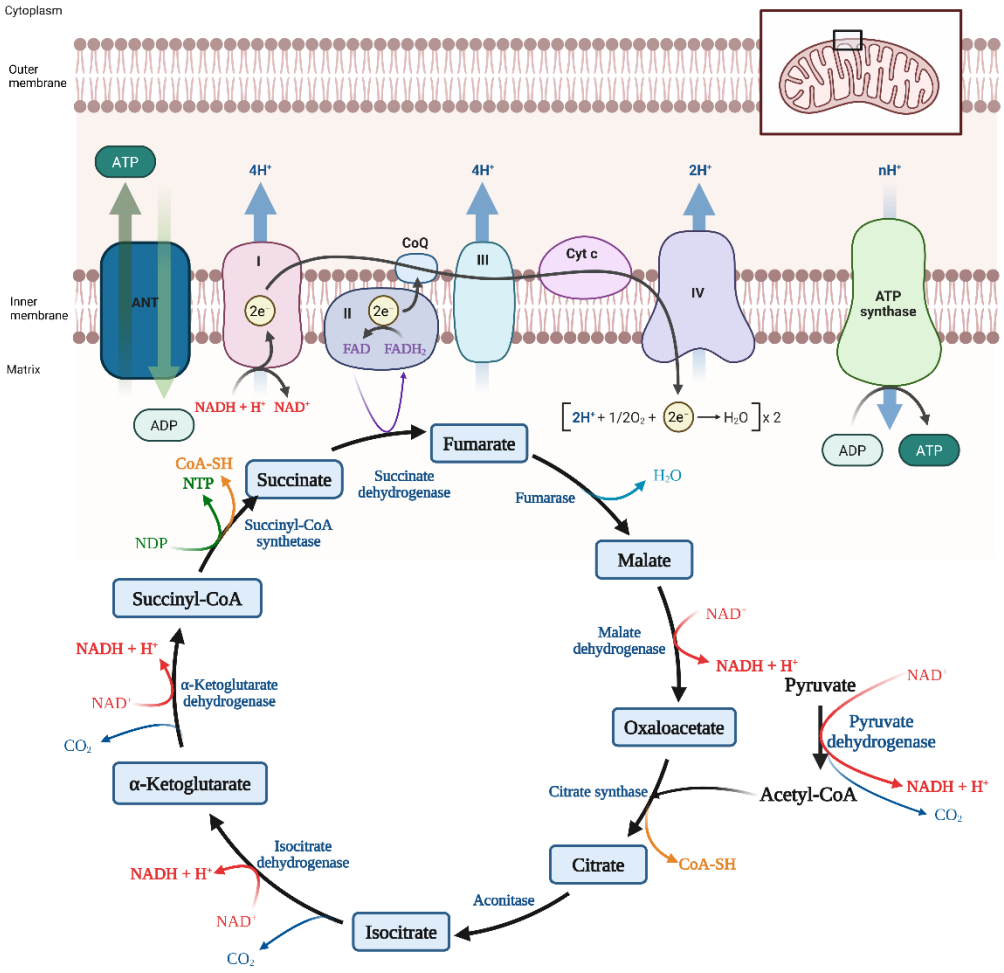

Figure 1. Connections between the TCAc and ETS. The TCAc and PDHc generate NADH for CI. SDH (aka CII) uses its FAD prosthetic group to support the ETS. Succinyl-CoA synthetase produces NTP (ATP or GTP) via substrate-level phosphorylation (SLP)

The alpha-ketoglutarate dehydrogenase complex

The KGDHc (also known as 2-oxoglutarate dehydrogenase complex, OGDHc, EC 1.2.1.105) is one of the most crucial enzymes in oxidative metabolism, located in the mitochondrial matrix. The enzyme catalyses the oxidative decarboxylation of α-ketoglutarate (α-KG) into succinyl-CoA, while NAD^+ is reduced and CO_2 is released (26). The enzyme complex is composed of three types of subunits (Fig. 2): α-ketoglutarate (or oxoglutarate) dehydrogenase (*KGDH/OGDH*, E1k, EC 1.8.1.4), dihydrolipoyl (or dihydrolipoamide) succinyltransferase (*DLST*, E2k, EC 2.3.1.61), and dihydrolipoyl (or

dihydrolipoamide) dehydrogenase (*DLD*, E3, EC 1.8.1.4) (27-29). While E1k is unique to KGDHc, E2k is shared between KGDHc and alpha-ketoadipate dehydrogenase, while E3 is the common subunit for alpha-ketoacid dehydrogenases (namely PDHc, branched-chain alpha-ketoacid dehydrogenase complex and alpha-ketoadipate dehydrogenase complex) and the glycine cleavage system (30). Although the exact subunit ratio of mammalian KGDHc is still obscure, the best proposed composition is an E1k:E2k:E3 subunit ratio of 24:24:12 (31). Furthermore, succinyl-CoA, which is produced by the KGDHc, will be the substrate for the TCAc-related substrate-level phosphorylation (SLP) reaction, which is catalysed by the succinyl-CoA ligase (the enzyme has 2 isoforms and can produce either ATP or GTP) and which becomes the primary energy source when OXPHOS is inhibited (e.g. hypoxia) (32, 33). Not only the product of the KGDHc-catalysed reaction, but the substrate, α-KG, is also an important molecule in many signalling pathways (see the sections below and (34)).

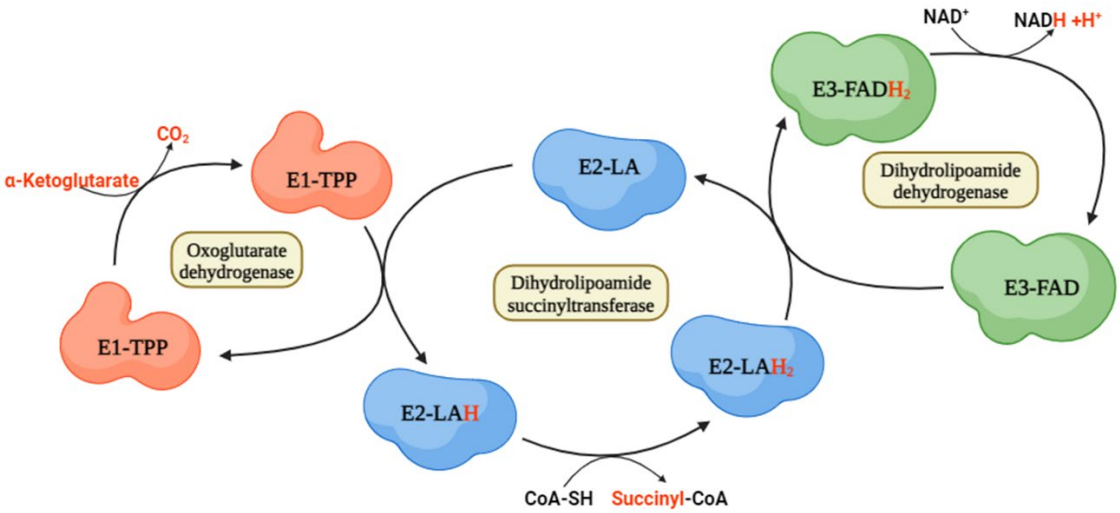

Figure 2. Structure of KGDHc. The complex has 5 cofactors/prosthetic groups: thiamine pyrophosphate (TPP), lipoic acid (LA), Coenzyme A (CoA), FAD and NAD^+

KGDHc and ROS

KGDHc is a controversial enzyme in many aspects. One of them is its Janus-faced properties related to ROS (34, 35). ROS are unavoidable byproducts of aerobic metabolism, particularly within mitochondria. At physiological concentrations, typically in the lower nanomolar range, ROS behave as signalling molecules, primarily through the oxidation of specific cysteine residues in target proteins; this process is referred to as

"oxidative eustress", which was first described by Helmut Sies (36, 37). Just like the original stress conception proposed by Hungarian-born János Selye (38), the oxidative stress thesis states that ROS can have positive effects on cellular homeostasis, although only intermittently and as previously mentioned, only at low concentrations. If ROS concentrations increase, cells undergo numerous pathological changes, hence the term "oxidative distress" is established (39).

When molecular oxygen (O_2) is reduced with a single electron, it becomes superoxide ($O_2^{\cdot-}$). The superoxide anion radical is very reactive; it can be spontaneously (or enzymatically by superoxide dismutase, SOD) converted into hydrogen peroxide (H_2O_2), which is also a member of the group collectively termed ROS (40). Hydrogen peroxide does not spontaneously degrade but can be degraded via the catalase and glutathione peroxidase catalysed reaction (catalase: $2\ H_2O_2 \rightarrow 2\ H_2O + O_2$ glutathione peroxidase: $2\ GSH + H_2O_2 \rightarrow GSSG + 2\ H_2O$) or by the Haber-Weiss reaction ($O_2^{\cdot-} + H_2O_2 \rightarrow OH^- + OH^{\cdot} + O_2$) when free iron ions are available to enhance the Fenton reaction ($Fe^{2+} + H_2O_2 \rightarrow Fe^{3+} + OH^- + OH^{\cdot}$) (41, 42). However, ROS are highly reactive molecules, thus they can quickly interact with macromolecules, such as lipids, proteins, and nucleic acids and therefore these molecules lose their original function (43). The above-mentioned radicals are strong prooxidant agents, hence they catalyse the peroxidation of lipids, which leads to a vicious cycle and results in membrane dysfunction (44). Moreover, ROS can react with nitrogen and sulphur-containing groups and molecules and the products are reactive nitrogen species (RNS) and reactive sulphur species (RSS) (45, 46).

Superoxide and hydrogen peroxide are two oxygen-derived species with significant physiological and pathophysiological roles in cellular signalling pathways. These oxygen derivatives have effects on the regulation of processes such as antioxidant and stress responses, cell proliferation and differentiation, the maintenance of ion gradients and pH homeostasis, as well as a variety of catabolic and anabolic reactions (47, 48). There are many factors that contribute to oxidative stress; including inherited and acquired (or somatic) mutations, environmental effects (e.g. toxins or irradiation), and random changes in the concentration of metabolites (15).

Multiple sites contribute to the generation of ROS, with NADPH oxidases and mitochondria representing the principal sources (47, 49). Mitochondrial ROS production

was first described by Jensen in 1966 (50). Over following 60 years, researchers have identified at least twelve sites inside the mitochondria which can produce ROS under given circumstances (15, 47).

Undeniably, parts of the ETS (CI, CII, CIII) are important sites in ROS production. Briefly, CI can generate ROS under three circumstances. The first is a commonly used Parkinson's disease model, which was described by the Greenamyre group (51); when rotenone (rot) is added to the mitochondria, it blocks the complex near the ubiquinone-binding site. After supplementing the complex with NADH-producing substrates (pyruvate, glutamate, or malate) the rate of H_2O_2 generation was elevated (52). Of note, to initiate this kind of ROS production, the NAD(P)H/NAD(P)$^+$ ratio must be high. Second, when mitochondrial membrane potential ($\Delta\Psi_m$) is high and CI substrate is provided, the complex can generate measurable amounts of ROS in the forward reaction because the redox centres are highly reduced (53, 54). The third condition is the reverse electron transfer (RET) (55). When $\Delta\Psi_m$ is high (the membrane is hyperpolarized) and the coenzyme Q pool is highly reduced (ubiquinol/ubiquinone, QH_2/Q, ratio is elevated) the electrons flow backward in the ETS from QH_2 into CI, hence generating excessive ROS. In this scenario, NAD$^+$ will be the final electron acceptor, hence the NADH/NAD$^+$ ratio is increased, and this condition can provoke further ROS production on the E3 subunit of ketoacid dehydrogenases, like KGDHc (more details below) (56, 57). NAD$^+$ is not obligatory for RET; however, it boosts the ratio of ROS formation (58). Succinate (Succ, S) oxidation in the absence of ADP and/or rot can generate robust ROS, via RET on CI (59). It is important to point out that RET-induced ROS is more sensitive to $\Delta\Psi_m$ than ΔpH (60). Chouchani theorised that RET may play a key role in the ischaemia-reperfusion (IR) injury (61). IR injury is described as an additional tissue injury after the occluded artery (ischaemia) was reopened (reperfusion). The above-mentioned research suggests that during ischaemia, Succ has reached four times higher concentration than the pre-ischaemic concentration. Of note, other TCAc metabolites do not show any similar accumulation. Initially during reperfusion, Succ is oxidised on CII, and the electrons are transferred to QH_2 via reduced $FADH_2$. Due to the high $\Delta\Psi_m$, electrons can be transferred backward, via RET to CI, while enormous amounts of ROS are produced (Fig. 3). IR injury is still an unsolved problem in common situations like stent placement after

myocardial infarction (62). Additional damage to the injured tissue can lead to further necrosis in the penumbra.

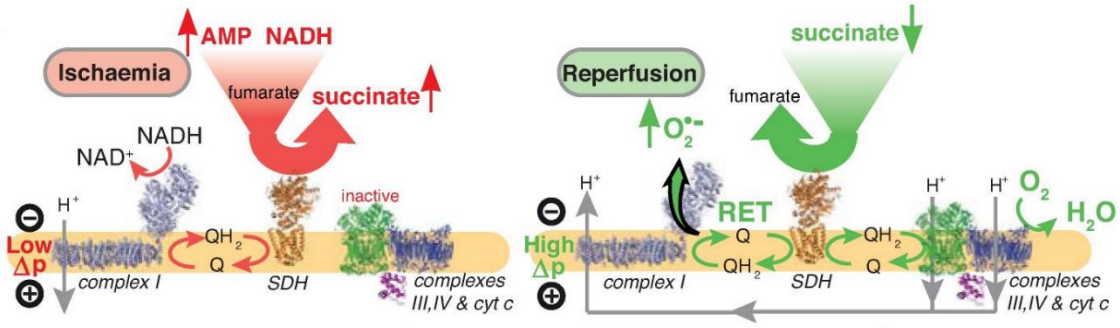

Figure 3. Importance of RET in IR injury. Succinate is accumulated during anoxia and the very beginning of reperfusion, electrons flow backward to CI via RET, accordingly, generating high amounts of ROS (for more detailed information check the text above). Source (with permission): Chouchani ET, Pell VR, Gaude E, et al. Ischaemic accumulation of succinate controls reperfusion injury through mitochondrial ROS. Nature. 2014; 515(7527): 431-435. doi:10.1038/nature13909 (61)

As previously mentioned, an increased ratio of $NADH/NAD^+$ favours the O_2^- production on the flavin prosthetic group of E3 subunit. Under this condition, KGDHc tends to produce more ROS in rat skeletal muscle mitochondria compared to the CI (63). The role of KGDHc in ROS generation is still questioned even in the scientific world. Importantly, in rat skeletal muscle mitochondria, when each enzyme was examined under its optimal conditions, the KGDHc exhibited the highest rate of ROS production among the α-keto acid dehydrogenase complexes (63). The isolated, intact KGDHc can generate superoxide, which can undergo spontaneous dismutation to form H_2O_2, in both the forward (physiological) and reverse directions of its catalytic activity (30, 56, 64, 65). NAD^+ suppresses ROS formation in both directions of the reaction and restores the enzyme to its physiological catalytic mode. In the reverse direction, the isolated KGDHc generated ROS upon addition of NADH in the absence of TPP and CoA. When substrates and cofactors were present, the ROS production was more dependent on the changes of the $NADH/NAD^+$ ratio for the KGDHc (56, 57, 63). This circumstance may enhance the importance of KGDHc derived ROS in IR injury, since this pathophysiological condition is associated with an elevated $NADH/NAD^+$ ratio. The production of ROS in KGDHc is mostly attributed to the E3 subunit (66, 67). Nonetheless, evidence suggests that isolated

human E1k or E1k-E2k subcomplexes can also generate ROS under given circumstances (65, 68). Notably, KGDHc is not only a source, but also as a target of ROS (35, 64). The covalently bound lipoic acid (LA) cofactor in E2k is irreversibly inactivated by H_2O_2 and by end products of lipid peroxidation (69, 70). Additionally, LA can be reversibly inactivated by glutathionylation or nitrosylation (71, 72). During this process, the sulfhydryl (–SH) group of the lipoamide cofactor in its reduced form (LAH_2) is susceptible to oxidation by reactive oxygen species, leading to the generation of a thiyl radical (RS·). This radical species subsequently reacts with reduced glutathione to form a transient thiyl radical-glutathionyl intermediate (RSSG·–) which in turn reacts with molecular oxygen to yield a disulfide bridge with the protein-bound sulfhydryl group.

KGDHc in diseases

Homozygous or compound heterozygous mutations affecting the KGDHc are frequently associated with rare autosomal recessive disorders (73-75). Acute manifestations of these conditions are typically characterized by metabolic decompensation and severe lactic acidosis, which predominantly result in neurological, hepatic, and cardiac complications (76-79). Among the above-mentioned conditions, E3 deficiency represents the most severe form, as the *DLD* subunit is a shared component of five distinct enzyme complexes (further details in the sections above). This deficiency is frequently characterized by neonatal onset and is commonly associated with early mortality (76, 80).

In the last few decades, many neurodegenerative diseases have been more accurately characterised via animal models and *postmortem* analyses of human samples. The results highlight that abnormalities in KGDHc activity can (at least partially) lead to pathological changes in the central nervous system. However, we cannot exclude the possibility that KGDHc activity is not a cause but a consequence of these pathological conditions in human patients. (Table 1., (31)).

Table 1. Pathological conditions and diseases related to KGDHc malfunction.

Source (slightly modified from the original): Hansen GE, Gibson GE. The α-Ketoglutarate Dehydrogenase Complex as a Hub of Plasticity in Neurodegeneration and Regeneration. Int J Mol Sci. 2022;23(20):12403. doi:10.3390/ijms232012403 (31). For further information and original sources check the cited article.

Name of the pathological condition	Attribute	Result of analysis
Infantile lactic acidosis	Extreme psychomotor retardation	Deficiency and mutations in E3
Psychomotor retardation (in childhood)	Mental & physical slowing	Disruption of E2k function
Intermittent neuropsychiatric disease with ataxia	attention deficit disorders, mild ataxia, lack of coordination and hypotonic weakness	G229C mutation in E3
Friedreich's ataxia	Damage to the long tracts in the spinal cord and development of ataxia	GAA repeats cause defect in the FRDA gene, deficiency in E3
Parkinson's disease	Secondary motor function is impaired, decline in intelligence	Dysfunction of the E2k, reduced KGDHc activity
Huntington's disease	Movement disorder followed by cognitive deficits	Reduced KGDHc activity
Alzheimer's disease	Loss of memory and cognitive function	Reduced KGDHc activity
Progressive supranuclear palsy	Postural instability and cognitive impairment	Reduced KGDHc activity in superior frontal cortex and cerebellum

Spinal cord injury	injury-associated behavioural changes such as depression and cognitive decline	Reduced KGDHc activity in spinal cord (by 90 %) and in cerebral cortex by 30 %
Wernicke Korsakoff Syndrome	Severe memory deficits	Reduced KGDHc activity

KGDHc distribution in the central nervous system

Establishing direct correlations between KGDHc activity and neurological disorders remains challenging. These complexities are further exacerbated by differences in KGDHc expression and activity among brain regions. In rat brain, cerebral cortex has the highest activity, after that the cerebellum, midbrain, striatum and hippocampus; the lowest activities were measured in hypothalamus, pons, medulla and *bulbus olfactorius* (81). In 2020, Dobolyi and his colleagues discovered that in human cerebral cortex KGDHc is expressed exclusively in neurons (82). This finding strengthens earlier results where loss of KGDHc activity was linked to neuronal death in Alzheimer's disease (AD) from human *postmortem* samples (83) and an earlier suggestion in the literature about neuronal preponderance of KGDHc (84). Of note, in rodent models slightly detectable KGDHc activity can be found in astroglia and significantly higher activity in neurons (85). Moreover, the laboratory of Waagepetersen and Schousboe hypothesized a completely working TCAc in the rodent astrocytes, thus they propose the presence of KGDHc in the brain of these animals (86, 87).

It is important to point out the fact that even a truncated TCAc can play a crucial role in brain metabolism via glutamine-glutamate cycle (88, 89). The glutamine–glutamate cycle was recognized long ago inside the brain (90). Initially, following the uptake of glutamate from the synaptic cleft, astrocytes convert it into glutamine by glutamine synthetase, while utilising one ATP molecule and one free ammonia (Fig. 4). Subsequently, neurons absorb the extracellular glutamine released by astrocytes, reconvert it into glutamate by the glutaminase enzyme and package it into synaptic vesicles (91, 92). Inside the neurons, a portion of glutamate can be metabolized into α-KG, thus entering the TCAc and producing ATP via OXPHOS. Neuronal energy metabolism is primarily based on the catabolism of glucose into pyruvate, which enters the mitochondria and supplies the TCAc. Glutamate is typically reserved for

neurotransmission and is not commonly utilized as a metabolic substrate. However, under conditions in which mitochondrial pyruvate availability is limited or TCAc is inhibited proximally to KGDHc (i.e. aconitase inhibition by H_2O_2) or any pathological condition disrupts the physiological flow of the TCAc, glutamate can serve as an alternative energy source (93, 94). It is essential to remove glutamate from the synaptic cleft, otherwise glutamate would stimulate N-methyl-D-aspartate (NMDA) receptors for a prolonged period, leading to glutamate-induced neurotoxicity (95).

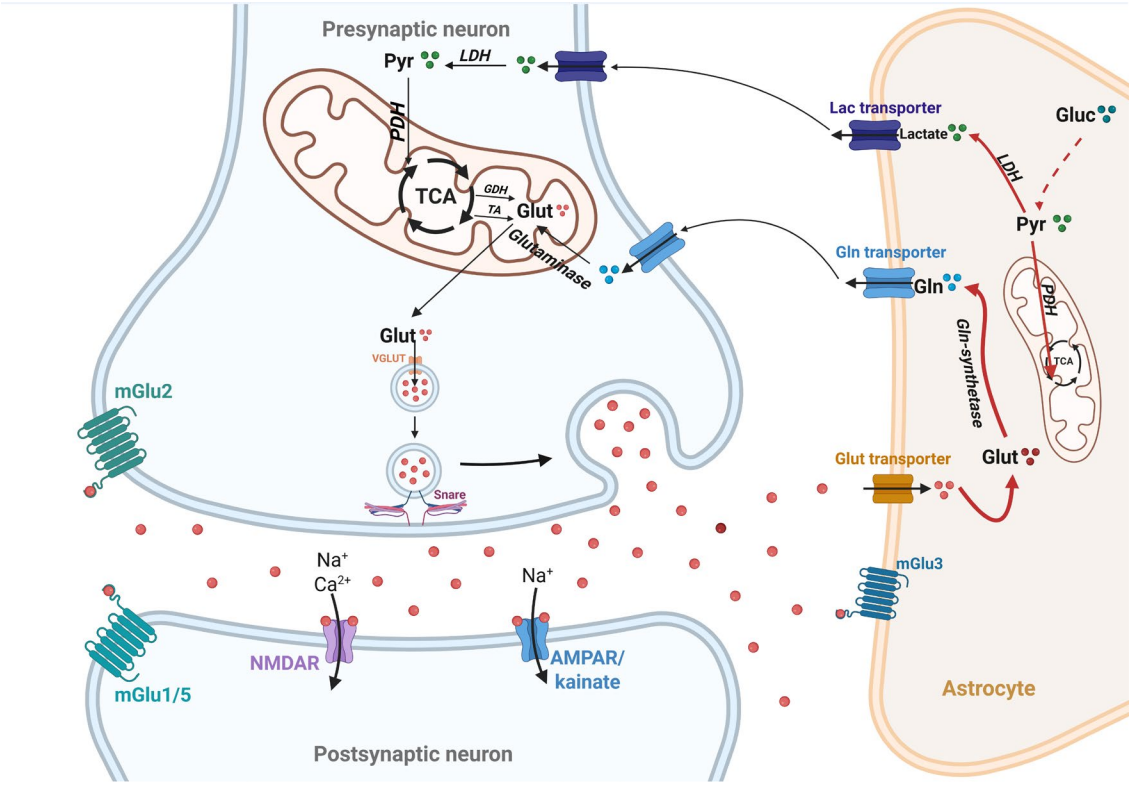

Figure 4. Glutamine-glutamate cycle in the brain. Neurotransmitter glutamate (Glut) is released from the presynaptic neuron and binds to the postsynaptic cation channels (AMPA/kainate or NMDA). After that, glutamate is taken up by astrocytes, where it is transformed into glutamine (Gln), then transported back to the presynaptic neuron. There, glutamate is synthesised from Gln by glutaminase or from α-KG by glutamine dehydrogenase (GDH) and transamination (TA).

II. Objectives:

Our aim was to investigate the metabolic consequences of KGDHc dysfunction *in vivo* and *in vitro* using *DLST* and *DLD* double heterozygous knockout (*DLST*$^{+/-}$-*DLD*$^{+/-}$, DKO) mouse strains. Our specific questions were as follows:

- How does combined *DLST*$^{+/-}$-*DLD*$^{+/-}$ heterozygosity influence the KGDHc related mitochondrial bioenergetics such as mitochondrial oxygen consumption, ATP synthesis rate and ROS production in isolated mitochondria?
- Is there any compensatory upregulation of certain TCAc-related enzymes?
- Does this genetic alteration influence body composition or amino acid and fatty acid profile in the blood?
- Do DKO mice possess altered endurance in a fatigue test?
- Is this genetic modification accompanied by any cognitive deficit and neurological alterations?
- Are there any histological or PET-CT imaging alterations of different tissues between DKO and wild-type (WT) mice?
- Are there any age-dependent differences in mitochondrial bioenergetics, metabolic parameters, and neurological alterations in this DKO mouse strain compared to WT animals?

III. Methods:

Animals

The heterozygous $DLD^{+/-}$ (C57BL/6) mice and their WT littermates were obtained from The Jackson Laboratory (Bar Harbor, ME, USA). Heterozygous $DLST^{+/-}$ mice (C57BL/6 and 129SV/EV hybrid background) and their WT littermates were provided by Lexicon Pharmaceuticals, Inc. (The Woodlands, TX, USA). Double heterozygous $DLD^{+/-}$/$DLST^{+/-}$ mice were generated in-house by crossbreeding $DLD^{+/-}$ and $DLST^{+/-}$ strains. Male mice aged 100–150 days (WT100, DKO100) and 200–250 days (WT200, DKO200) were used in all experiments. Animals were maintained under minimal disease (MD) conditions in a controlled environment (20–22 °C, 12-hour light/dark cycle, 65 % relative humidity). Mice were fed a standard rodent chow diet consisting of 55 % carbohydrates, 27 % protein, and 7 % fat, and had ad libitum access to food and water. All experimental procedures were conducted in accordance with the International Guiding Principles for Biomedical Research Involving Animals and Guidelines for Animal Experiments at Semmelweis University according to the EU Directive "Directive 2010/63/EU of the European Parliament and of the Council of 22 September 2010 on the protection of animals used for scientific purposes". All procedures and experiments were approved by the Animal Care and Use Committee of the Institute of Experimental Medicine and the Animal Health and Food Control Station, Budapest (permission numbers: PE/EA/00957-6/2024 and PE/EA/00960-4/2024). All experiments were performed with the experimenter/operator blinded to the genotype of the animals.

Genotyping

Genomic DNA suitable for polymerase chain reaction (PCR) was isolated from mouse samples using the hot sodium hydroxide and pH adjustment with a Tris solution (HotSHOT) method as described by Truett (96). PCR amplification was performed using conventional protocols in a total reaction volume of 20 µL, containing 2 µL 10× DreamTaq Buffer, 1 µM of each primer (wild type, mutant and common), 0.25 mM deoxynucleotide triphosphate, 0.5 U DreamTaq Green DNA Polymerase, and 2 µL template DNA (approximately 15 µg/mL). All PCR reagents were obtained from Thermo Fisher Scientific (Waltham, MA, USA). Oligonucleotide primers were purchased from Sigma-Aldrich and Life Technologies and are listed in Table 2. DNA samples were subjected to thermal cycling for heterozygous $DLD^{+/-}$ mice as follows: initial denaturation

at 95 °C for 2 min followed by 35 cycles at 94 °C for 30 sec, 61.5 °C for 60 sec and 72 °C for 60 sec, with a final extension of 72 °C for 7 min. For heterozygous $DLST^{+/-}$ mice, the cycle conditions were as follows: initial denaturation at 95 °C for 2 min followed by 30 cycles at 94 °C for 30 sec, 55.0 °C for 30 sec and 72 °C for 40 sec, with a final extension at 72 °C for 7 min.

Table 2. Oligonucleotide sequences for genotyping

Primer designation	Sequence	PCR product (bp)
Dld wild type	CAT GGC TCC TTT CAG CTG TT	340
Dld common	ACA ATA TAC CCG CCT CAC CA	
Dld mutant	TCG CCT TCT TGA CGA GTT CT	232
Dlst wild type	ATAAACCCTCTTGCAGTTGCATC	186
Dlst common	TAGGTTCCTAGGTAGGGATACAGC	
Dlst mutant	CTACTCTCTAACCTACCAAGCTGG	210

Animal sacrifice and blood sample collection

Animals received intraperitoneal (i.p.) heparin (5000 U/kg; Ratiopharm GmbH, Ulm, Germany) to prevent coagulation, followed 3 minutes later by i.p. administration of ketamine–xylazine anaesthesia (80/4 mg/kg; CP-Pharma Handelsgesellschaft GmbH, Burgdorf, Germany). Adequate depth of anaesthesia was confirmed by the absence of a motor response (paw withdrawal reflex) to a noxious stimulus, assessed by paw pinch using atraumatic forceps (97). Blood samples (~0.5 mL) were collected via the retro-orbital sinus. A single drop of whole blood was applied for dried blood spot (DBS) preparation, while the remaining sample was centrifuged at 1500*g* for 10 minutes at 4 °C. The resulting serum was collected and stored at −80 °C until further analysis. Subsequently, the thoracic cavity was opened, the right atrium was incised, and mice were transcardially perfused with ice-cold phosphate-buffered saline (PBS) via the left ventricle.

Amino acid and acylcarnitine profiles in mouse dried blood spots (DBS) were determined by electrospray ionization tandem mass spectrometry (ESI–MS/MS) on a Sciex Triple Quad 3500 system (Sciex, Framingham, MA, USA), employing a non-kit derivatization approach as previously described (98). Amino acid quantification from mouse serum samples was performed using the MassChrom® Amino Acids LC-MS/MS kit (Chromsystems, Gräfelfing, Germany) on a QTRAP 4500 LC-MS/MS system (Sciex, Framingham, MA, USA), in strict accordance with the manufacturer's specifications.

mRNA expression analysis

Total RNA was isolated from liver tissue using the Direct-zol™ RNA Miniprep Plus Kit in accordance with the manufacturer's protocol (Zymo Research, Irvine, CA, US). Total RNA (1 µg) from each sample was used to prepare cDNA with an oligo-dT primer by single-strand reverse transcription (RevertAid First Strand cDNA Synthesis Kit, Thermo Fisher Scientific, Waltham, Massachusetts, US). Gene expression was analyzed via quantitative real-time PCR using the Power SYBR Green PCR Master Mix (Life Technologies, Carlsbad, CA, US) and an Applied Biosystem QuantStudio 12K Flex Real-Time PCR system (ThermoFisher Scientific) (Aranyi & Tusnady, 2007 (99)). Reactions were carried out in 96-well plates with a final volume of 10 µL, following the manufacturer's instructions. Relative mRNA quantification was performed using the 2^{-dCt} method and normalizing to ribosomal protein 29 (Rps29). All reactions were carried out in duplicate. The gene-specific primers are listed in Table 3.

Table 3. Gene-specific primers used for mRNA expression

Gene	Forward (5' ->3')	Reverse (5'->3')
Glutamate dehydrogenase 1	GCTAAAGCAGGCGTTAAGA	TCAATGCCAGGACCAATAAA
α-ketoglutarate dehydrogenase (E1k)	CAACTCAGATGACCCTGAAG	GTCGATAACACACCAGATCAA
Dihydrolipoamide dehydrogenase (E3)	GCTTGAACGTTGGTTGTATTC	TCAAGCGAACTTCTGGTATTT
Dihydrolipoamide succinyltransferase (E2k)	CTTCAGGGTTCGCTTCTTC	GCATCTCCAACAGCTTTCT
Pyruvate carboxylase	CAGAGGAGTTTGAGGTTGAG	GAAGCTGCCCATTGAGTT
ATP citrate:lyase	GGGAGGAAGCTGATGAATATG	GTCAAGGTAGTGCCCAATG
Branched-chain alpha--ketoacid dehydrogenase (E1b)	CCAGGGATCAAGGTGGTAATA	TGCTGCCCGGTAAAGTAT
Succinate dehydrogenase complex, subunit A	CAAGACTGGCAAGGTTACTT	TCATCAGTAGGAGCGGATAG
Ribosomal protein S29	CGGTCTGATCCGCAAATAC	GGTCGCTTAGTCCAACTTAAT

Isolation of brain and kidney mitochondria

Mitochondria were isolated from young and middle-aged male mouse brains using a discontinuous Percoll gradient, as previously described (60, 100, 101). Following dissection, brains were rapidly removed and placed in ice-cold Buffer A (in mM: 225 mannitol, 75 sucrose, 5 HEPES, 1 EGTA; pH 7.4). Tissue samples were minced and homogenized using a glass/Teflon Potter-Elvehjem homogenizer. The homogenate was first centrifuged at 1300*g* for 3 minutes, and the resulting pellet was discarded. The supernatant was subsequently centrifuged at 20,000*g* for 10 minutes. The resulting pellet was resuspended in 15 % Percoll and layered onto a discontinuous Percoll gradient consisting of 23 % and 40 % fractions. The suspension was centrifuged for 8 minutes at 30000*g*. The mitochondrial fraction was accumulated and collected from between the 23 % and 40 % Percoll layers, then it was resuspended in ice-cold Buffer A and centrifuged again at 16600*g* for 10 minutes. After that, the pellet was resuspended again in Buffer A and recentrifuged at 6300*g* for 10 minutes. Thereafter, pellet was resuspended in ice-cold Buffer B (in mM: 225 mannitol, 75 sucrose, 5 HEPES, pH 7.4) yielding ~ 30 mg/mL mitochondrial protein concentration.

Isolation of kidney mitochondria was performed as described earlier by Fernández-Vizarra et al. (102), with minor modifications. Briefly, kidneys were excised and surrounding connective tissue and the renal capsule were removed. Wet tissue mass was determined using blotting paper. The tissue was then minced into small pieces with sharp scissors in ice-cold isolation Buffer C (in mM: 220 sucrose, 70 mannitol, 10 EGTA, 2 HEPES; pH 7.4) and washed in the same buffer to remove residual blood. Afterwards, the tissue was homogenized with a Dounce homogenizer and then centrifuged at 900*g* for 10 min. The supernatant was then centrifuged at 15,000*g* for 5 min. Next, the supernatant was discarded, the pellet was resuspended in ice-cold isolation Buffer C (10 mL/g wet tissue) and transferred into two Eppendorf tubes and centrifuged twice at 15,000*g* for 5 min. Finally, the pellet was resuspended in 75 µL isolation Buffer C, yielding a mitochondrial protein concentration of approximately 40 mg/mL. All procedures were performed on ice or at 4 °C, and mitochondria were used within 4 h of resuspension.

The mitochondrial protein concentration was determined using a modified Biuret assay (103, 104).

Western blot analysis

Pellets of isolated mitochondria from WT and DKO mice were resuspended in radioimmunoprecipitation assay (RIPA) buffer containing 10 mM Tris/HCl (pH 7.4), 1% NP-40, 0.1% sodium deoxycholate, 0.1% SDS, and 150 mM NaCl, supplemented with a protease inhibitor cocktail (P8340-5 mL). After 20 s sonication (Sonopuls HD 2070 probe sonicator, Bandelin electronic GmBH & Co. KG, Berlin, Germany) experiments were carried out on ice, cycle interval was 15 s, power amplitude was 10%, the mitochondrial debris was removed by centrifugation at 14,000*g* and 4 °C for 10 min. Protein concentrations in the resulting supernatants were determined using the bicinchoninic acid (BCA) assay with bovine serum albumin (BSA) as the standard. 10 µg protein samples were denatured for 5 min at 95 °C, then loaded on a non-reducing 10% polyacrylamide gel. After size separation by electrophoresis at 140 V, proteins were transferred to a nitrocellulose membrane for 15 min (Trans-Blot Turbo Blotting System, Bio-Rad, Hercules, CA, USA). Transfer efficiencies were assessed *via* Ponceau staining. Membranes were blocked for 1 hour at room temperature (RT) in Tris-buffered saline with Tween-20 (TBST; 20 mM Tris, 150 mM NaCl, pH 7.4, 0.05% Tween-20) containing 5 % non-fat milk and 0.5 % BSA. Primary antibodies against E1k (ab137773), E2k (ab177934), and E3 (ab133551) were purchased from Abcam (Cambridge, UK), and the antibody against Complex IV (CIV; 4850T) was obtained from Cell Signaling Technology (Danvers, MA, USA). Primary antibodies were diluted in TBST and incubated with the membranes overnight at 4 °C. After washing three times for 10 min in TBST, membranes were incubated with horseradish peroxidase-conjugated anti-rabbit IgG secondary antibodies (Enzo Life Sciences, Farmingdale, NY, USA) diluted 1:5,000 in TBST for 1 h at room temperature. Following an additional three TBST washes, signals were developed with ECL reagent (Bio-Rad, Hercules, CA, USA) for 2 min and detected using a gel documentation system (Syngene, Cambridge, UK). CIV immunoblotting was used for normalization of protein expression levels, and densitometric analysis was performed using ImageJ. The primary antibodies were used in the following dilution ratios: E1k – 1:1,000, E2k – 1:10,000, E3 – 1:10,000, CIV – 1:1,000.

Respiratory medium

Mitochondrial oxygen consumption, H_2O_2 production, and ATP generation were all monitored in a respiratory buffer containing (in mM) 125 KCl, 20 HEPES, 2 KH_2PO_4, 0.1 EGTA, 1 $MgCl_2$ and 0.025% fatty-acid free BSA, pH 7.4.

Mitochondrial oxygen consumption

Mitochondrial oxygen consumption was measured by high-resolution respirometry using an Oroboros Instruments system (Innsbruck, Austria) at 37 °C in 2-mL chambers under continuous stirring at 750 rpm (105). Oxygen concentration was monitored with a polarographic oxygen sensor (POS) and recorded using DatLab 7.4 software (Oroboros Instruments). The POS was calibrated daily at air saturation and routinely at zero oxygen in oxygen-depleted medium, and instrumental background oxygen flux measurements were performed periodically. Oxygen fluxes were calculated in real time as the negative time derivative of oxygen concentration and corrected for instrumental background flux, dilution caused by titrations, and residual oxygen consumption measured in the presence of mitochondria in the absence of ADP or respiratory substrates, all within DatLab 7.4. Mitochondria were used at a concentration of 0.05 mg/mL and energized with either α-ketoglutarate (5 mM) or succinate (10 mM) to determine leak respiration. Subsequently, saturating ADP (2.5 mM) was added to assess OXPHOS capacity.

Mitochondrial ATP production

Mitochondrial ATP generation rate was determined using a coupled-enzyme assay based on hexokinase (HK) and glucose-6-phosphate dehydrogenase (G6PDH), as previously described (106, 107). The respiratory medium (2 mL total volume) was supplemented with 2.75 mM glucose, 1.65 mM $NADP^+$, 1.1 U G6PDH, 4.4 U HK, and 150 µM P1,P5-di(adenosine-5′)-pentaphosphate (AP5), an adenylate kinase inhibitor. Upon provision of respiratory substrates and ADP, mitochondria synthesized ATP, which was exported to the extramitochondrial compartment via the adenine nucleotide translocase. In the extramitochondrial medium, the exported ATP served as the phosphate donor for HK-catalysed phosphorylation of glucose to glucose-6-phosphate, which was subsequently oxidized to 6-phosphogluconate by G6PDH, coupled to the stoichiometric reduction of $NADP^+$ to NADPH. NADPH production was monitored spectrophotometrically at 340 nm and 37 °C using a JASCO V-650 spectrophotometer (ABL&E-JASCO, Tokyo, Japan), and the resulting absorbance signal (ε = 6,220

$L \cdot mol^{-1} \cdot cm^{-1}$) was taken as a direct measure of ATP efflux from mitochondria. The assay was calibrated against known ATP standards (100 µM). Mitochondria (0.05 mg/mL) were energized with either α-KG (5 mM) or succinate (10 mM), which was followed by ADP (2.5 mM) addition to induce ATP production. Then, oligomycin (25 nM) was added to inhibit OXPHOS *via* the inhibition of the ATP-synthase. At the end, FCCP (carbonyl cyanide-p-trifluoromethoxyphenylhydrazone, 25 nM), an uncoupler, was administered to measure SLP.

Mitochondrial ROS generation

Mitochondrial H_2O_2 production was assessed using the Amplex UltraRed fluorescence assay, as previously described (60, 108). Horseradish peroxidase (2.5 U/mL), Amplex UltraRed reagent (2 µM), and mitochondria (0.1 mg/mL) were added to the respiratory medium. Fluorescence was recorded at excitation and emission wavelengths of 550 nm and 585 nm, respectively, using a PTI Deltascan fluorescence spectrophotometer (Photon Technology International, Lawrenceville, NJ, USA) at 37 °C. At the end of each experiment, the fluorescence signal was calibrated with a known H_2O_2 standard (100 pmol), and H_2O_2 fluxes were expressed relative to the background flux measured in the presence of mitochondria alone. All measurements were performed in an open cuvette at air saturation (~190 µM O_2). H_2O_2 production by kidney mitochondria was monitored in the presence of 100 µM phenylmethyl sulfonyl fluoride (PMSF), which is an inhibitor of carboxylesterases. According to Miwa (109), carboxylesterases may convert Amplex UltraRed to the fluorescent end product, resorufin requiring no HRP, O_2, or H_2O_2, leading to fluorescent artifacts.

TCAc enzyme activity assays

Enzyme-activity measurements were carried out in 50 mM KH_2PO_4, pH 7.4 applying mitochondria at 0.1 mg/mL; traces were recorded with a JASCO V-650 spectrophotometer. The results were calculated using the theoretical molar extinction coefficient from the literature for NAD(P)H, ε=6,220 $dm^3 \cdot mol^{-1} \cdot cm^{-1}$. Aconitase activity was determined spectrophotometrically as previously described (93, 110). Briefly, the assay medium was supplemented with 2 mM EGTA, 3 mM $MgCl_2$, 0.6 mM $MnCl_2$, 0.1% (v/v) Triton X-100, and 0.281 U $NADP^+$-dependent IDH, followed by the addition of mitochondria. The reaction was initiated by the addition of 0.5 mM $NADP^+$ and 10 mM citrate, and NADPH formation was monitored at 340 nm. Overall KGDHc activity was

assessed spectrophotometrically following a previously established protocol with minor modifications (81, 93). The assay medium contained 2 mM EGTA, 3 mM $MgCl_2$, 0.2 mM thiamine pyrophosphate, 2.5 mM ADP, 2 mM NAD^+, 1 μM rot, 0.1% (v/v) Triton X-100, and mitochondria. The reaction was initiated by the addition of 5 mM α-KG and 0.12 mM CoA, and NADH formation was monitored at 340 nm.

Determination of body composition

Whole-body composition was assessed prior to metabolic measurements using quantitative magnetic resonance (EchoMRI 700 Whole Body Composition Analyzer; E26-233RM, Echo Medical Systems, Houston, TX, USA).

Determination of metabolic parameters

Animals were singly housed for one week prior to the commencement of experiments. Two days before metabolic measurements, mice were transferred to the test cages of a TSE PhenoMaster indirect calorimetry system (TSE Systems, Berlin, Germany) to allow acclimatization to the measurement environment and familiarization with the drinking bottles and feeders. Key metabolic variables — including food and water intake, three-dimensional (X-Y-Z) locomotor activity, O_2 consumption, and CO_2 production — were automatically recorded at 15-minute intervals over a continuous 24-hour period (111). The respiratory exchange ratio (RER) was calculated as the ratio of CO_2 production to O_2 consumption.

Treadmill fatigue test

Prior to the fatigue test, animals underwent a two-day treadmill acclimatization protocol, as previously described (112). On the first day, mice were allowed to freely explore the treadmill apparatus for 1–3 minutes, after which the belt was activated and speed was gradually increased to 8 m/min. Speed was subsequently raised to 9 m/min at 5 minutes and to 10 m/min at 7 minutes, with the session terminated at 10 minutes. On the second day, following a brief exploratory period, belt speed was progressively increased to 11 m/min at 5 minutes and to 12 m/min at 10 minutes, with the session concluded at 15 minutes. On the third day, the fatigue test was initiated at a belt speed of 12 m/min, which was thereafter incrementally increased according to the protocol outlined in Table 4.

Table 4. Treadmill speed as a function of time

Time (min)	Speed (m/min)
0.5	14
1	16
6	18
30	20
45	22
60	24
75	26

Animals were immediately removed from the treadmill upon remaining continuously within the fatigue zone — defined as the rear section of the belt, approximately one body length from the electric grid — for five consecutive seconds (Fig 5).

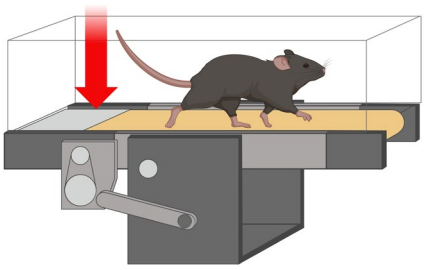

Figure 5. Schematic drawing of the treadmill. The red arrow indicates the fatigue zone, remaining in this zone for 5 s was defined as exhaustion.

Echocardiography

Cardiac function was evaluated by echocardiography using a Vevo 3100 high-resolution imaging system (Fujifilm VisualSonics, Toronto, Canada) equipped with an MX400 transducer. Mice were anaesthetized with isoflurane (5% for induction, 2% for maintenance) and placed on a heating pad to maintain physiological temperature. Core temperature was continuously monitored via rectal thermometry, and heart rate (HR) was assessed by concurrent electrocardiography. All measurements were performed in accordance with previously established protocols (113) and international echocardiographic standards (114). Left ventricular (LV) end-diastolic and end-systolic volumes (LVEDV and LVESV, respectively) were derived from two-dimensional long-

axis views. Short-axis imaging was used to obtain end-diastolic and end-systolic LV internal diameters (LVIDd and LVIDs, respectively), as well as LV anterior and posterior wall thicknesses in both diastole and systole (LVAWd, LVAWs, LVPWd, and LVPWs, respectively). Diastolic function parameters — including early mitral valve peak inflow velocity (E), early diastolic mitral annular velocity (e'), and isovolumetric relaxation time (IVRT) — were assessed by Doppler imaging in the apical four-chamber view. Derived cardiac functional indices were calculated as follows:

$$SV = LVEDV - LVEDS$$

$$EF = {}^{SV}/_{LVEDV} \times 100$$

$$Cardiac\ output = SV \times HR$$

$$FS = {}^{(LVIDd - LVIDs)}/_{LVIDd}$$

$$LVmass = 1.053 \times [(LVIDd + LVAWd + LVPWd)^3 - LVIDd^3] \times 0.8$$

$$LVremodelling\ index = {}^{LVmass}/_{LVIDd}$$

The abbreviations are as follows: stroke volume (SV); ejection fraction (EF); fractional shortening (FS). All echocardiographic recordings were analysed using VevoLAB software (Fujifilm VisualSonics, Toronto, Canada).

Cognitive tests

Open field test

The open field test (Fig 6a) was employed to evaluate horizontal and vertical locomotor activity, anxiety-like behaviour, and exploratory drive, as previously described (115). The apparatus consisted of a circular arena 80 cm in diameter, subdivided into 20 subsectors by concentric and radial lines and enclosed by a 35 cm high aluminium wall. Each animal was individually placed at the centre of the arena, and psychomotor behaviour was assessed by direct visual observation over a 5-minute period. Horizontal locomotor activity was quantified by the number of line crossings performed during ambulation, while vertical activity was determined by the frequency of rearing events. Anxiety-like behaviour was inferred from the relative time spent in the inner versus outer zones of the arena. To prevent olfactory carry-over between successive trials, the arena

was thoroughly cleaned with 70 % (v/v) ethanol and dried with absorbent paper towels between individual tests.

Novel object recognition tests

Novel object recognition (NOR, Fig 6b) was assessed in the same open field arena one day following the open field test, according to established protocols (116, 117). During the sample trial, two identical objects were positioned symmetrically relative to each other but asymmetrically relative to the centre of the arena, at equal distances from the wall. Animals were permitted to freely explore both objects for 5 minutes, after which they were removed from the arena and returned to their home cage. Following a 120-minute inter-trial interval, a test trial was conducted in which one of the previously presented objects was replaced with a novel object of distinct shape and texture. Animals were again allowed to explore both objects for 5 minutes. The total number of visits (visit frequency) and the cumulative time spent per visit at each object were recorded in seconds. Cognitive recognition performance was quantified using a recognition index (RI), calculated as follows:

$$RI = \frac{Tnovel}{Tnovel + Tfamiliar} \times 100$$

where $Tnovel$ and $Tfamiliar$ denote the total duration of visits to the novel and familiar objects, respectively, and RI is expressed as a percentage.

Morris water maze test

The Morris water maze test (Fig 6c) is an experimental test to examine the spatial learning capacity of animals (118). The test was conducted in a circular, black-walled water tank (diameter: 153 cm, height: 63 cm) filled to a depth of 53 cm with water maintained at 24 ± 1 °C. A circular escape platform (diameter: 10.8 cm), painted black to minimize visual contrast with the tank, was submerged at a fixed location 1.5 cm below the water surface. Animals were tested over five consecutive days, with one session per day, each comprising four trials initiated from different starting positions distributed around the perimeter of the tank, presented in varying order across trials. Each trial was terminated upon successful location of the platform by the animal. If the platform was not located within the 90 second maximum trial duration, the animal was manually guided to and placed on the platform by the experimenter. Following each trial, the animal remained

on the platform for 30 seconds before being removed. Escape latency — defined as the time elapsed from trial onset to platform location — was recorded in seconds for each trial. Within each daily session, the latency of the first trial was designated as a measure of reference memory, while the mean latency across all four daily trials was used as an index of working memory.

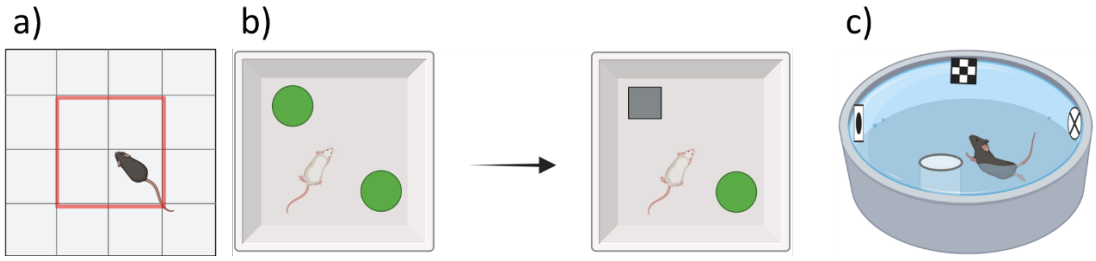

Figure 6. Schematic drawing of cognitive tests. Open field test (a); novel object recognition tests (b); Morris water maze test (c)

Histology

Mouse brains were fixed in 4 % (v/v) phosphate-buffered formaldehyde for 24 hours at room temperature (25 °C), subsequently dehydrated through a graded alcohol series, and embedded in paraffin. Serial sections of 5 µm thickness were prepared using a rotary microtome (HistoCore MULTICUT, Leica Biosystems, Nussloch, Germany) for immunohistochemical analysis. Sections were deparaffinized in xylene (2 × 10 min), rehydrated through a descending alcohol series, and subjected to heat-induced epitope retrieval at pH 9 and 95 °C for 30 minutes. Nonspecific protein binding was reduced by 5 % skimmed milk in Tris-buffered saline solution. Sections were then incubated with primary antibodies for 1 hour at room temperature, followed by incubation with horseradish peroxidase-conjugated secondary antibodies for 1 hour at room temperature. Each step was preceded and followed by three Tris-buffered saline washes (3 × 5 min, room temperature). Antibody labelling was visualized using 3,3′-diaminobenzidine (DAB) as the chromogenic substrate. Staining intensity was quantified using the H-score method, calculated as:

$$H\text{-}score = (\%\, weak \times 1) + (\%\, medium \times 2) + (\%\, strong \times 3)$$

where the percentage of the stained area exhibiting weak, medium, or strong intensity is weighted accordingly. H-score values range from a minimum of 0 to a maximum of

300. Neuronal and glial cells were distuinguished by a senior pathologist on the basis of morphological characteristics. he following primary antibodies were used: Anti-CD-68 polyclonal antibody (dilution: 1:500; 25747-1-AP, PTG labs, Manchester, UK), anti-PGC1A (dilution: 1:100; (66369-1-Ig, PTG labs, Manchester, UK), anti-Nrf2 antibody (dilution: 1:100; 16396-1-AP, PTG labs, Manchester, UK), anti-DRP1 antibody (dilution: 1:100; 12957-1-AP, PTG labs, Manchester, UK), anti-MFN2 antibody (dilution: 1:100; 12186-1-AP, PTG labs, Manchester, UK), anti-mTFA antibody (dilution: 1:100; ab307302, AbCam, Cambridge, UK). Secondary antibodies: Rabbit IgG VisUCyte HRP Polymer Antibody (VC003-050, R&D Systems, Inc, MN), Mouse IgG VisUCyte HRP Polymer Antibody (VC001-050, R&D Systems, Inc, MN), DAB (Vector Labs, Redcar, UK). Skeletal muscle samples from the musculus quadriceps femoris were prepared using routine formalin fixation and paraffin embedding method (see above). The sections were 5 µm thick and stained with haematoxylin and eosin for histological estimation; sections were examined for extensive necrosis, inflammation, or fatty degeneration. Sirius red stain (Thermo Fischer Scientific) was also applied to detect evidence of fibrosis. The sections were stained with sirius red stain (PanReac AppliChem, Darmstadt, Germany) for 1 h at RT, then the samples were washed twice with acidified water (0.5 v/v % acetic acid) and finally, the sections were dehydrated with pure (96 v/v %) ethanol and cleared with xylene.

PET-CT

A volume of 0.18 ± 0.09 mL [^{18}F]-fluorodeoxyglucose (FDG, activity of 9.39 ± 1.25 MBq; means ± SD) was administered intravenously into the lateral tail vein. Mice were anesthetized with isoflurane (1.5%) for the whole duration of imaging with CT and PET (nanoScan SPECT/CT and nanoScan PET/MRI -3T; Mediso, Hungary). Helical CT scan settings: 50 kVp and 980 uA, 300 ms experimental time, 1:4 binning, pitch: 1, zoom factor: 1.2, 687 projections (360 projections/rotation). Static scans of 60-min duration were collected 10 min post-injection in an energy window of 400–600 keV. All PET images were reconstructed using the respective device's three-dimensional Maximum A Posteriori (MAP, P4 system) or three-dimensional Monte-Carlo-modelled Ordered Subsets Expectation Maximization (Tera-Tomo 3D-OSEM, Mediso, Hungary) algorithm, with corrections for dead time, scattering, and attenuation, where available. Reconstructed images of 0.3 mm voxel size were then visualized using the software

VivoQuant (inviCRO, USA) and Fusion (Mediso, Hungary), respectively. To assess energy consumption, we utilized the standardized uptake values (SUVs).

Chemicals

Unless otherwise specified, all chemicals were purchased from the Merck Group (Darmstadt, Germany). The following reagents and kits were obtained from alternative suppliers: Amplex UltraRed reagent and the RevertAid First Strand cDNA Synthesis Kit (both from Thermo Fisher Scientific, Waltham, MA, USA); Direct-zol™ RNA Miniprep Plus Kit (Zymo Research, Irvine, CA, USA); and Power SYBR Green PCR Master Mix (Life Technologies, Carlsbad, CA, USA).

Statistics

All statistical analyses were performed using GraphPad Prism 8.0 (GraphPad Software, San Diego, CA, USA). Data are presented as means ± S.E.M (unless indicated otherwise). Group differences were assessed by two-way analysis of variance (ANOVA) followed by Šídák's post hoc multiple comparisons test, as specified in the respective figure legends. Two factors were the genotype (WT, DKO) and age (100 or 200 day old). For comparisons between two independent groups, an unpaired two-tailed Student's t-test was applied.

IV. Results:

Expression of KGDHc subunits and overall activity of the DKO mice mitochondria

First, genetic modification was verified in WT and DKO mice, by analysis of mRNA and protein expression of the three types of KGDHc subunits. Additionally, overall *in vitro* KGDHc enzyme activity was also measured from brain mitochondria (119). The mRNA expression of E2k and E3 was significantly reduced in DKO mice relative to controls (Fig. 7), with decreases of 58% (protein) and 45% (mRNA) for E2k, and 55% (protein) and 46% (mRNA) for E3, respectively. Additionally, a slight but not significant reduction in E1k protein abundance was observed in DKO animals which is in line with our previous findings in single heterozygous DLST and single heterozygous DLD knockout mice (120). Notably, E1k mRNA levels remained unchanged across all genotypes examined. As anticipated, overall KGDHc enzymatic activity was significantly reduced by 45% in isolated brain mitochondria of DKO animals.

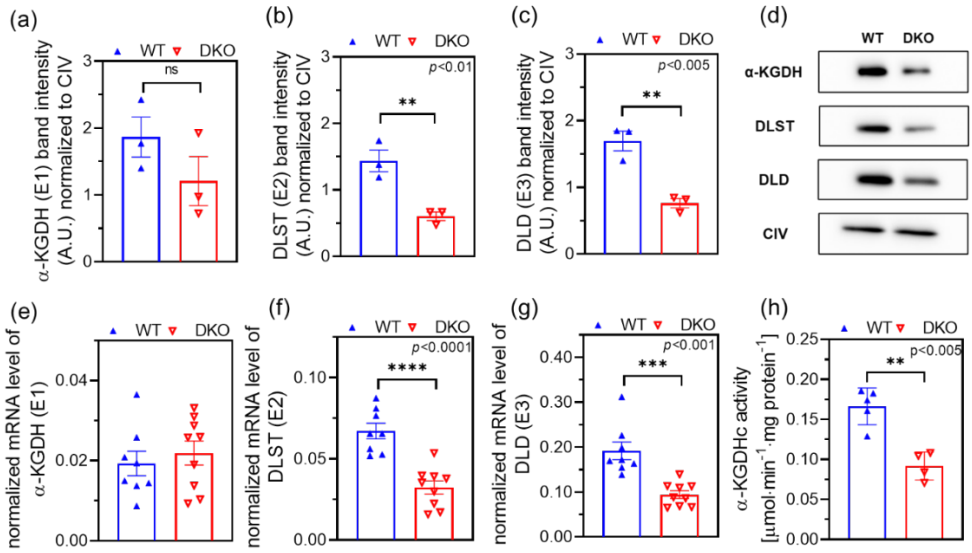

Figure 7. Western blot analysis of E1k (a), E2k (b), and E3 (c) protein expression and mRNA expression levels (e-g) in liver tissue of WT and DKO mice and overall KGDHc activity in isolated brain mitochondria (h). Band intensities were normalized to CIV expression (a-c). Representatives of immunoblot images are presented in panel (d). Relative mRNA levels of E1k (e), E2k (f), and E3 (g) in liver tissue, normalized to the housekeeping gene ribosomal protein S29. Statistical differences between groups were assessed using an unpaired Student's t-test. n = 3–9/group.

O_2 consumption and rate of ATP production in brain and in kidney mitochondria

In isolated mitochondria, distinct respiratory pathways can be selectively engaged through the exogenous provision of specific respiratory substrates, both in the presence and absence of ADP. In the present study, mitochondrial O_2 consumption (Fig. 8) and ATP synthesis rates (Fig. 9) were assessed in isolated brain and in kidney mitochondria energised with either the NADH-linked substrate α-KG or the $FADH_2$-linked substrate Succ. Following the addition of α-KG in the absence of ADP, LEAK respiration was monitored; no statistically significant differences were detected among the experimental groups under this condition. Subsequent addition of a saturating concentration of ADP was used to initiate α-KG-linked OXPHOS capacity, which was reduced by 43% in the DKO200 group and by 48% in the DKO100 group in the brain (Fig. 8b) and by 45 % in the DKO200 group but only by 19 % in the DKO100 group in the kidney (Fig. 8c) relative to their respective age-matched controls, which were not significant.

Succinate-linked respiration is conventionally assessed in the presence of the CI inhibitor rot, to prevent oxaloacetate accumulation arising from the activity of NADH-linked malate dehydrogenase. Oxaloacetate is a well-characterized inhibitor of succinate dehydrogenase, the accumulation of which results in the suppression of succinate-linked O_2 flux (121, 122). However, in the presence of rot, NADH accumulates and inhibits the formation of oxalacetate. As expected, Succ-induced O_2 flux, with or without ADP, did not significantly differ among the WT and DKO groups in both organs (Fig. 8e, f).

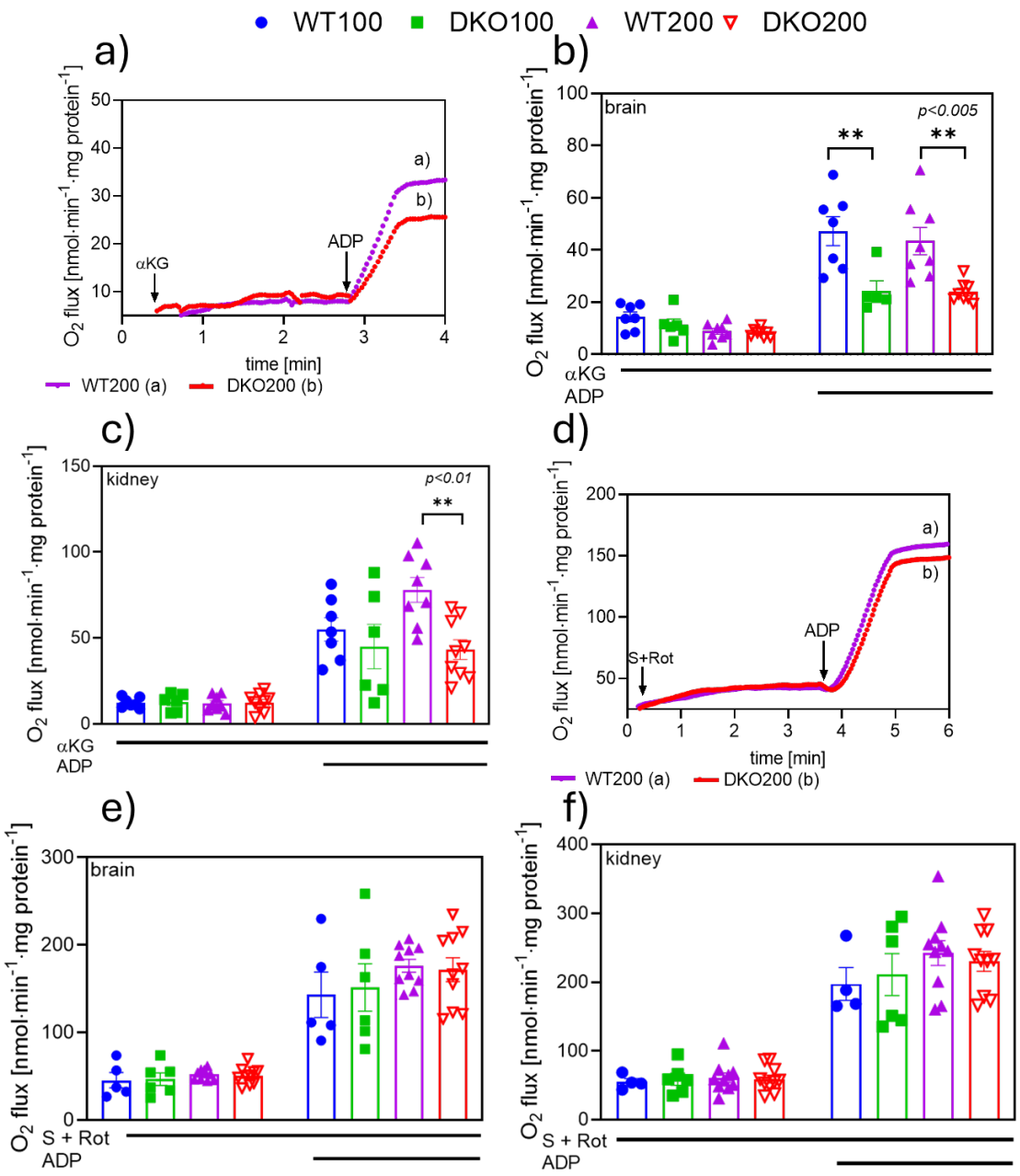

Figure 8. O_2 consumption of brain (b, e) and kidney (c, f) mitochondria.

Representative traces of independent experiments are shown in panel (a) using α-KG and (d) with Succ + rot in brain mitochondria. Blue circle - WT100: 100-150-day old WT mice; green square – DKO100: 100-150-day old DKO mice; purple triangles – WT200: 200-250-day old WT mice; open red triangles – DKO200: 200-250-day old DKO mice. Lines under the panels indicate additions of chemicals to the mitochondrial suspension. Data were analysed by two-way ANOVA. n = 5–10/group.

As anticipated, α-KG-linked ATP synthesis was significantly reduced in DKO mice relative to controls in the brain (Fig. 9b) (55 % reduction in DKO100; 40 % reduction in DKO 200). Surprisingly, in kidney mitochondria from young mice there were no significant differences between DKO100 and WT100 animals (Fig. 9c) and even in the middle-aged rodents, the reduction was only close to 20 %. Inhibition of ATP synthase by oligomycin markedly suppressed ATP production in all experimental groups, corroborating the predominant contribution of the F_oF_1-ATPase to mitochondrial ATP generation. Administration of the protonophore FCCP augmented ATP formation in brain to 187 % in the WT100, to 138 % in the DKO100, to 208 % in the WT200 and to 187 % in the DKO200 group, a response attributable to SLP driven by succinyl-CoA ligase in the brain (Fig. 9b) (107). In kidney, we could not detect any enhancement in the rate of ATP synthesis after administering FCCP (Fig. 9c).

In another set of experiments, Succ was employed as the respiratory substrate in the presence of rot (Fig. 9e, f). As anticipated, no statistically significant differences in Succ-linked OXPHOS capacity were detected in DKO mice relative to controls.

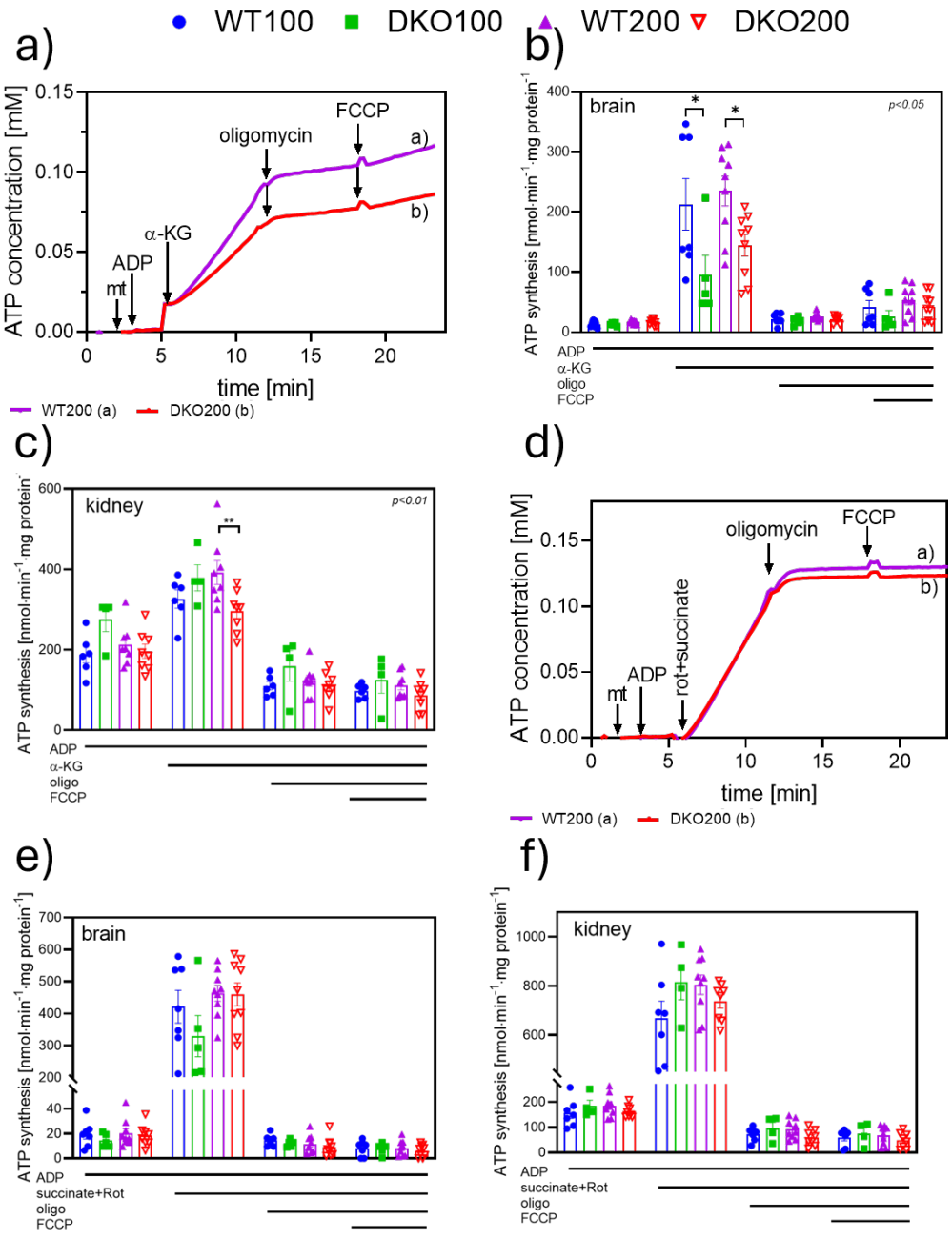

Figure 9. ATP production of brain (b, e) and kidney (c, f) mitochondria. Representative traces of independent experiments are shown in panel (a) using α-KG and (d) with Succ + rot in brain mitochondria. Lines under the panels indicate additions of chemicals to the mitochondrial suspension. Data were analysed by two-way ANOVA. n = 5–9/group.

Mitochondrial ROS production in brain and in kidney

The present study was primarily focused on H_2O_2 generation initiated by α-KG upon CI inhibition, as well as on Succ-induced RET-associated ROS production, given that RET represents a significant source of ROS during IR injury (61, 123). In isolated brain and kidney mitochondria respiring on α-KG, relatively low rate of H_2O_2 formation could be detected, which was attributed to the KGDHc and ETS (Fig. 10b, c). Under these conditions, no statistically significant difference was observed between the corresponding control and DKO groups. ADP exerted minimal effect on α-KG-induced H_2O_2 production across all experimental groups examined. Carboxyatractyloside (CAT), an ANT inhibitor, potentiated H_2O_2 generation, an effect attributable to hyperpolarization of $\Delta\Psi_m$. Rot significantly augmented H_2O_2 formation, a response that may be partially ascribed to enhanced ROS production at both CI and KGDHc, as a consequence of elevated NADH/NAD^+ ratio. Rot-induced H_2O_2 formation was reduced in brain by 62% and 44% in DKO100 and DKO200 animals (Fig. 10b), respectively, in kidney by 19% and 29% (Fig. 10c) relative to their corresponding age-matched controls. Antimycin A (Ama) enhanced the H_2O_2 production owing to the inhibition of the Qi site in CIII (15, 124).

Consistent with observations in *DLST* and *DLD* single KO mice, isolated mitochondria from DKO animals exhibited pronounced H_2O_2 generation upon energization with Succ in the absence of ADP, a response attributed to RET. RET-induced H_2O_2 production was reduced by 61 % and 63% (in brain, Fig. 10e) and by 34% and 47% (in kidney, Fig. 10f) in DKO100 and DKO200 animals, respectively, relative to their corresponding age-matched controls. Succ *plus* CAT enhanced the RET-induced H_2O_2 production in the middle-aged animals of both genotypes and both organs as compared to the corresponding younger groups, pointing to an age-specific increase in the RET (125).

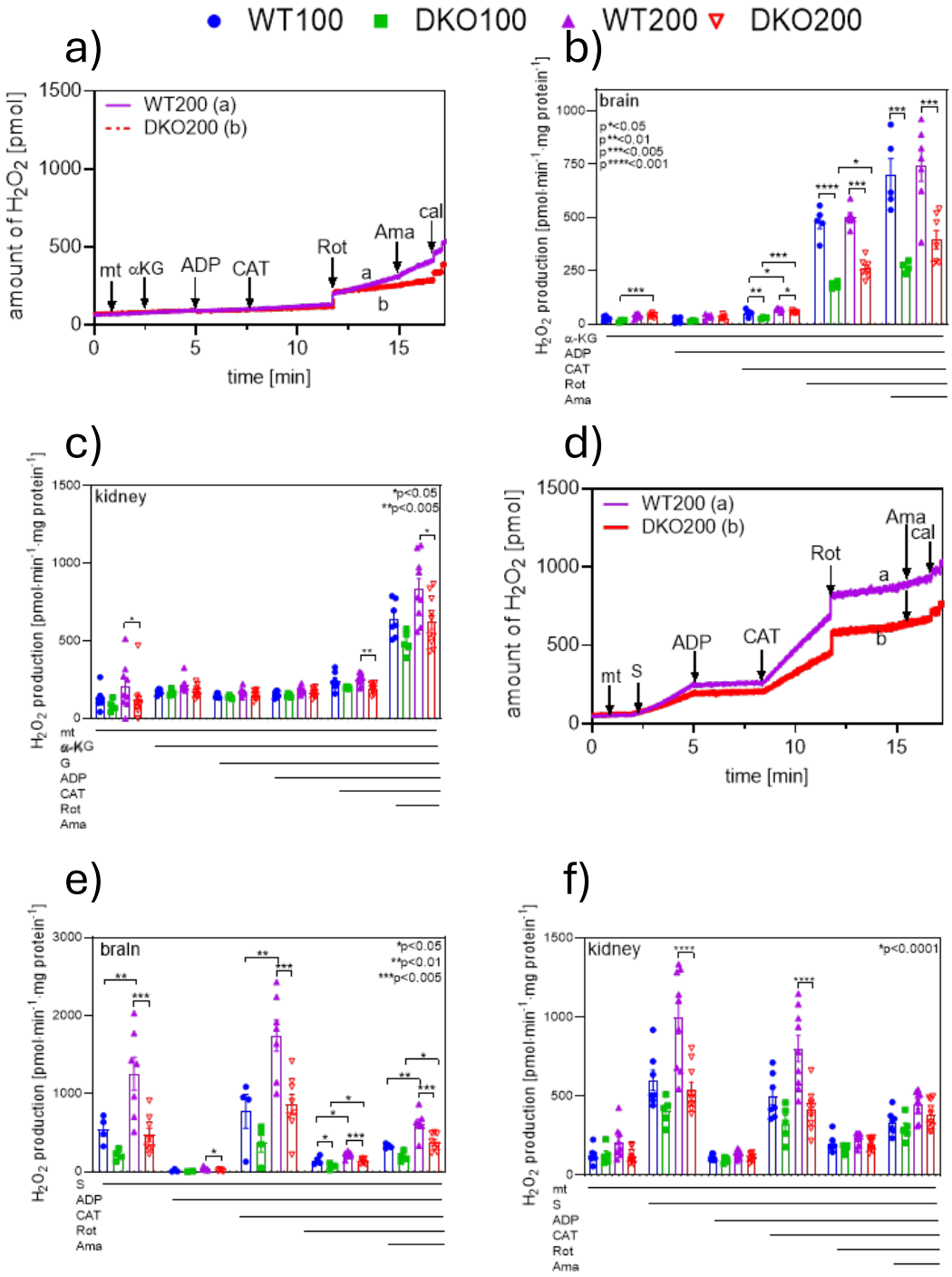

Figure 10. H_2O_2 production of brain (b, e) and kidney (c, f) mitochondria. Representative traces of independent experiments are shown in panels (a) and (d). Mitochondria were added to the respiratory medium after addition of Amplex UltraRed and HRP. Lines under the panels indicate additions of chemicals to the mitochondrial suspension. Data were analysed by two-way ANOVA. n = 4–9/group.

For further analysis of ROS generation, aconitase activity was measured after 15 min 10 mM Succ incubation in kidney mitochondria (Fig 11). It is well-known that aconitase, the most sensitive enzyme to H_2O_2 in the TCAc (93), compromised activity generally indicates accelerated H_2O_2 formation in the mitochondrion. Aconitase activity was 28 % higher in the DKO200 group compared to the age-matched WT.

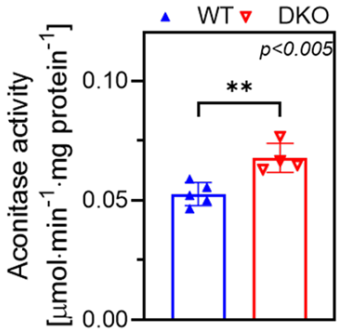

Figure 11. Aconitase activity in kidney mitochondria after a 15 min incubation with 10 mM Succ. The activity values were normalized to the citrate synthase activity. Data were analysed by the unpaired t-test. n = 9/group.

Compensation in the TCAc

Given that KGDHc is a key regulatory enzyme of the TCA cycle, its deficiency was anticipated to elicit compensatory upregulation of selected TCA cycle-related enzymes. Contrary to this expectation, hepatic mRNA levels of two anaplerotic enzymes – glutamate dehydrogenase and pyruvate carboxylase – remained unchanged in DKO mice relative to controls. Consistent with this observation, the mRNA level of SDH, which catalyses the TCAc reaction downstream of KGDHc, was likewise unaltered in DKO mouse liver. Furthermore, the mRNA level of cytosolic ATP-citrate lyase was not significantly different between DKO and control animals, indicating that citrate-dependent fatty acid synthesis was not augmented as a compensatory response to KGDHc deficiency.

Body composition, metabolic parameters, and amino acid/acylcarnitine profiling

Given the central role of the TCAc in cellular energy metabolism, a deficiency in KGDHc was hypothesized to affect body composition and overall body mass, potentially through alterations in nutrient utilization. Contrary to this expectation, no significant differences in total body mass (Fig. 12a), lean mass (Fig. 12b), or fat mass (Fig. 12c) were observed between age-matched DKO and WT animals, suggesting the absence of *in vivo* metabolic compensation under resting physiological conditions. Animals were additionally housed in metabolic cages to assess food intake (Fig. 12d), horizontal and

vertical locomotor activity (Fig. 12e), and RER (Fig. 12f). None of the previously mentioned parameter showed a significant difference between the age-matched groups, except locomotor activity. However, in another sets of experiments, these parameters were monitored under thermoneutral conditions (29-31 °C) and during the inactive phase of the rodent's circadian cycle (daylight) and there were no changes between genotypes (119).

Given that the catabolism of most amino acids and anabolism of fatty acids are linked to a functional TCAc or KGDHc activity, amino acid profiles were systematically analysed in serum and DBS from all experimental groups (119). No significant differences in amino acid profiles were detected between DKO and WT animals. The acylcarnitine profiles of these mice were also analysed from DBS samples to assess the mitochondrial fatty acid oxidation and utilization. No short-, medium-, or long-chain acylcarnitines differed between the DKO and control animals.

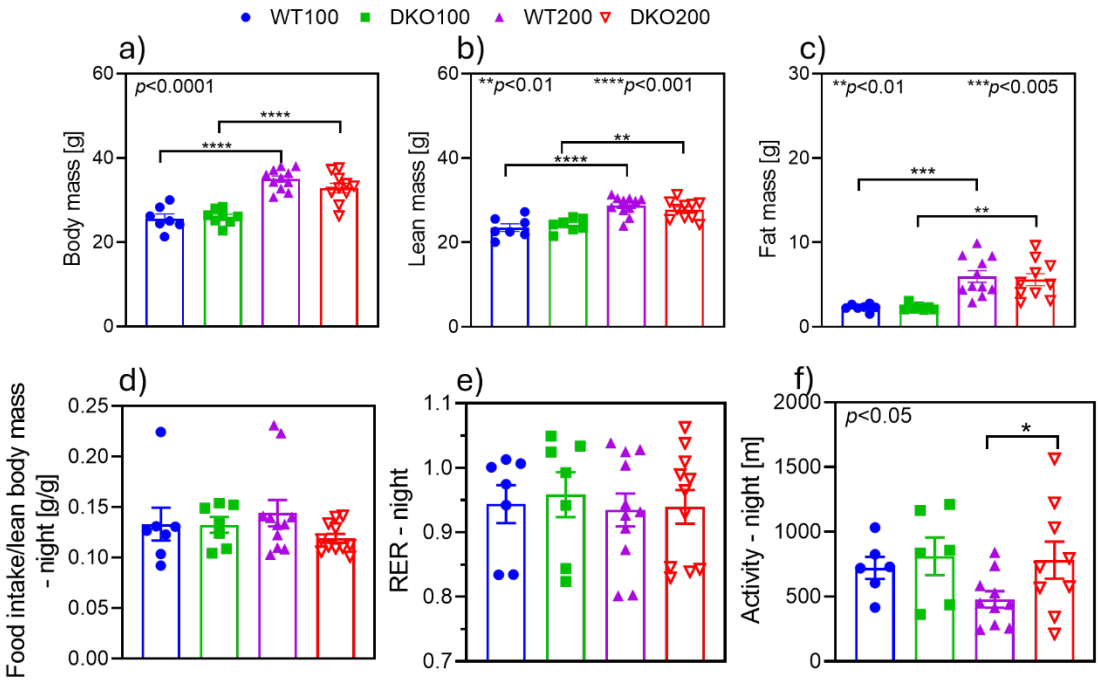

Figure 12. Body mass (a), body composition (b, c) and whole-body metabolic parameters (d-f) in four animal groups. Data were analysed by two-way ANOVA. n=6-11/group.

Forced endurance test

As was observed in previous experiments, the animals metabolically compensate well *in vivo* for a heterozygous double-knockout affecting the TCA cycle under resting circumstances. The question arose as to how the DKO mice would behave under a stress situation. The treadmill fatigue test was performed until full exhaustion on a motor-driven treadmill with increasing velocity (112). During the active phase (nocturnal period), DKO200 mice exhibited reductions in total running distance and time of 64.8% and 63.9%, respectively, relative to age-matched controls (Fig. 13a, c). These findings suggest that under conditions of KGDHc deficiency, the heightened energetic demands imposed by intense physical exercise cannot be adequately met, owing to impaired mitochondrial ATP synthesis and reduced O_2 utilization. During the inactive phase, DKO200 animals similarly demonstrated the poorest exercise performance relative to controls (Fig. 13b, d). In contrast, running performance in younger DKO animals was not significantly compromised relative to their respective controls.

We further hypothesized that fibrotic remodelling of skeletal muscle tissue may have contributed to the impaired exercise endurance observed in DKO mice. To address this, sirius red staining was applied to assess the degree of fibrosis in skeletal muscle sections (Fig. 13e-h). Histological examination of a minimum of four samples per experimental group revealed no evidence of fibrotic changes in DKO animals.

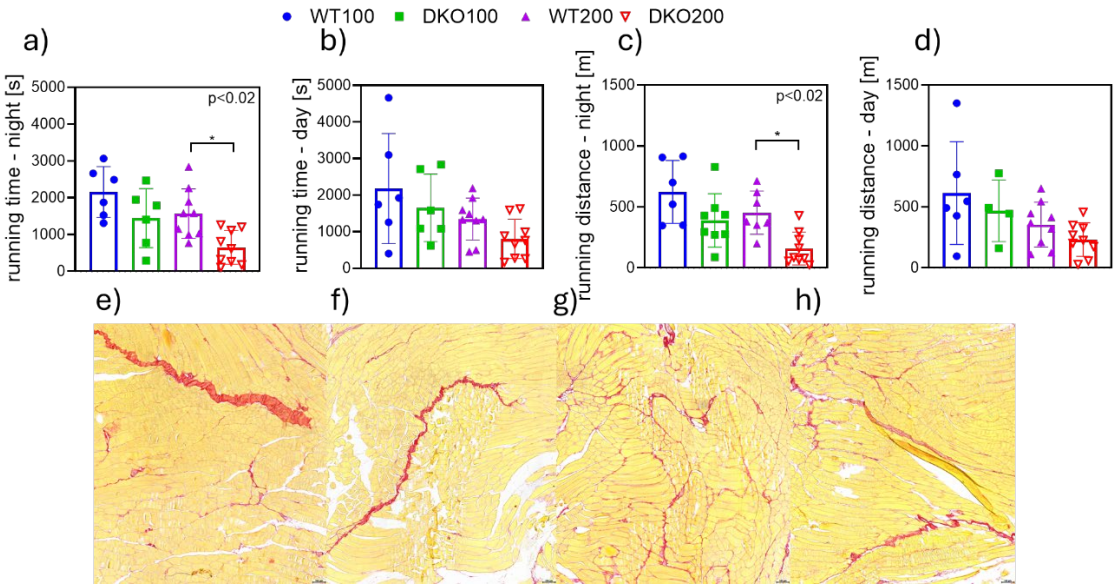

Figure 13. Results of the treadmill test (a-d) and Sirius red staining from histological samples of skeletal muscle (e-h). Running time (a, b) and distance (c, d) as well, were measured during both the active (a, c) and inactive (b, d) periods. Representative images of skeletal muscle samples from WT100 (e), DKO100 (f), WT200 (g) and DKO200 (h) mice. Data were analysed by two-way ANOVA. n=6-11/group

Cardiac dysfunction was considered as a potential contributing factor to the accelerated exhaustion observed in the forced treadmill test, and echocardiographic assessment was therefore performed (Fig. 14). Analysis revealed reductions in LVEDV (Fig. 14a) and SV (Fig. 14b) in younger DKO animals, which were accompanied by a significant decrease in CO in both mutant groups (Fig. 14d). EF (Fig. 14c) and FS (Fig. 14e), however, remained unaltered (mean heart rate was likewise unchanged). Diastolic function, as evaluated by IVRT (Fig. 14f) and the E/e' ratio (Fig. 14g), was found to be unaltered. Assessment of LVRI (Fig. 14h) and LV mass (Fig. 14i) did not reveal evidence of major cardiac structural remodelling.

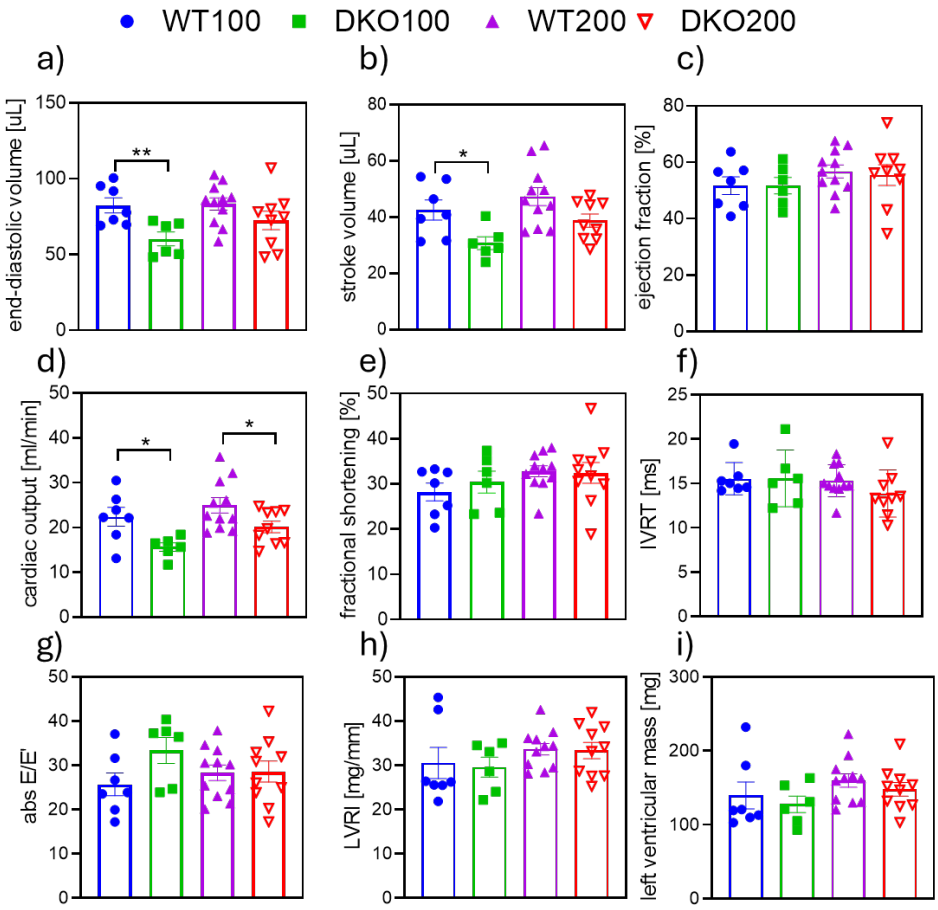

Figure 14. Echocardiographic measurements in four animal groups. Further details can be found in the above paragraph of the main text. Data were analysed by two-way ANOVA. n = 5–10/group.

Cognitive tests

KGDHc deficiency has been consistently associated with cognitive decline and impaired motor function in the literature (for review see (31)). However, no behavioural assessments have been reported in the context of KGDHc subunit-specific knockout animal models without administering (neuro)toxic chemicals (126, 127). To investigate whether compromised KGDHc activity can indeed lead to impairments in motor and cognitive functions, DKO and WT mice underwent various behavioural and memory tests.

In the open field test, novelty-induced horizontal locomotor activity, as quantified by the number of line crossings, was significantly reduced in both DKO100 and DKO200 groups relative to controls (Fig. 15a). Vertical activity, assessed by the frequency of rearing events, also exhibited a declining trend in DKO groups compared to controls (Fig.

15b). Nevertheless, the time spent in the inner and the outer zones of the arena did not differ between genotypes (Fig. 15c, d). The novel object recognition test (Fig. 15e, f) and the Morris water maze test (Fig. 15g, h) were conducted only with the middle-aged DKO mice to test their cognitive functions. The recognition index did not differ significantly between genotypes (Fig. 15f); however, total exploration time showed a tendency to be reduced in the DKO200 group (Fig. 15e). In the Morris water maze test, working memory was markedly impaired in DKO animals relative to controls (Fig. 15g), whereas differences in reference memory, although directionally consistent, remained only suggestive (Fig. 15h).

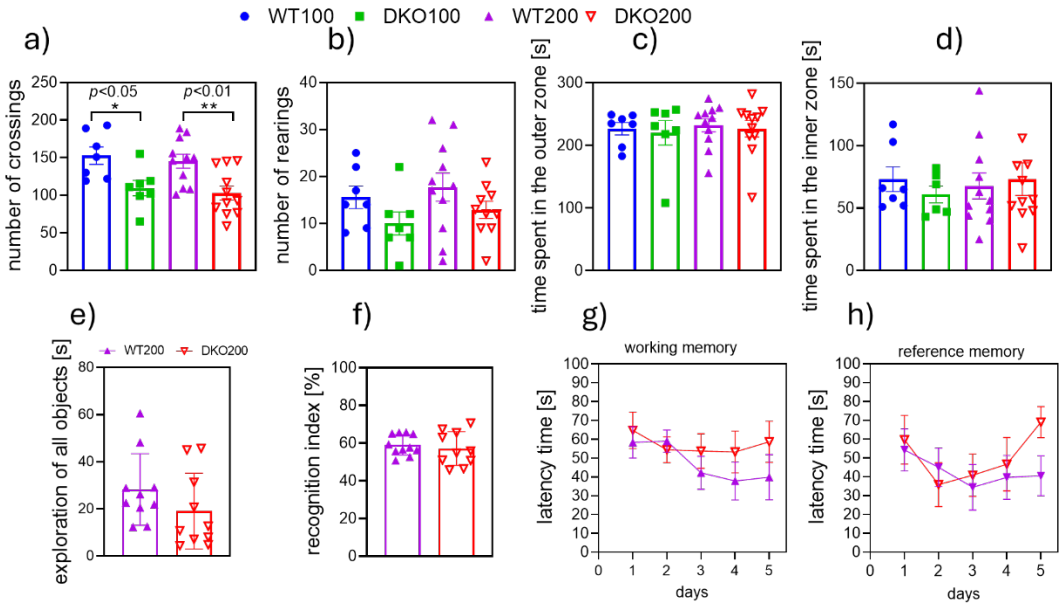

Figure 15. Results of cognitive tests. Further details can be found in the above paragraph of the main text. Data were analysed by two-way ANOVA; novel object recognition tests (e, f) were analysed by unpaired t-test. n = 6-11/group.

Microgliosis and neuronal death

To determine the origin of the changes observed in behavioural tests, histological samples were taken from different parts of the brain. CD68 (known as macrosialin in rodents) is a lysosome-associated membrane protein (LAMP) expressed predominantly in microglial cells within the brain (128). Expression of the CD68 antigen is upregulated in pro-inflammatory cytokine-activated macrophage-derived cells, including microglia,

but remains low in quiescent cells (129). Microgliosis is indicative of cortical neuronal damage arising from energy deprivation, which leads to the release of damage-associated molecular patterns (DAMPs) that subsequently trigger microglial activation (130, 131). In the cerebral cortex of the DKO200 mice (Fig. 16c, d), substantial microgliosis (WT200: 6.7±1, DKO200: 23.6±2 $CD68^+$ cells/visual field, at 40x magnification) was detected by CD68 immunostaining (Fig. 16i), pointing to neuroinflammation (132, 133).

Immunohistology samples from the hippocampal region were prepared using the terminal deoxynucleotidyl transferase-mediated dUTP-biotin nick end labeling (TUNEL) method. With this staining method, the terminal deoxynucleotidyl transferase specifically binds to the free 3'-OH end of DNA (134). Therefore, fragmented DNA leads to more binding sites, increasing the staining intensity. In aged DKO animals, the CA1 region of the hippocampus exhibited extensive DNA fragmentation (Fig. 16g, h) compared to age-matched controls (Fig. 16e, f). Notably, younger animals are expected to better tolerate intense proinflammatory signals, as described by other researchers (135). Consequently, the brains of young mice were not examined by immunohistochemistry.

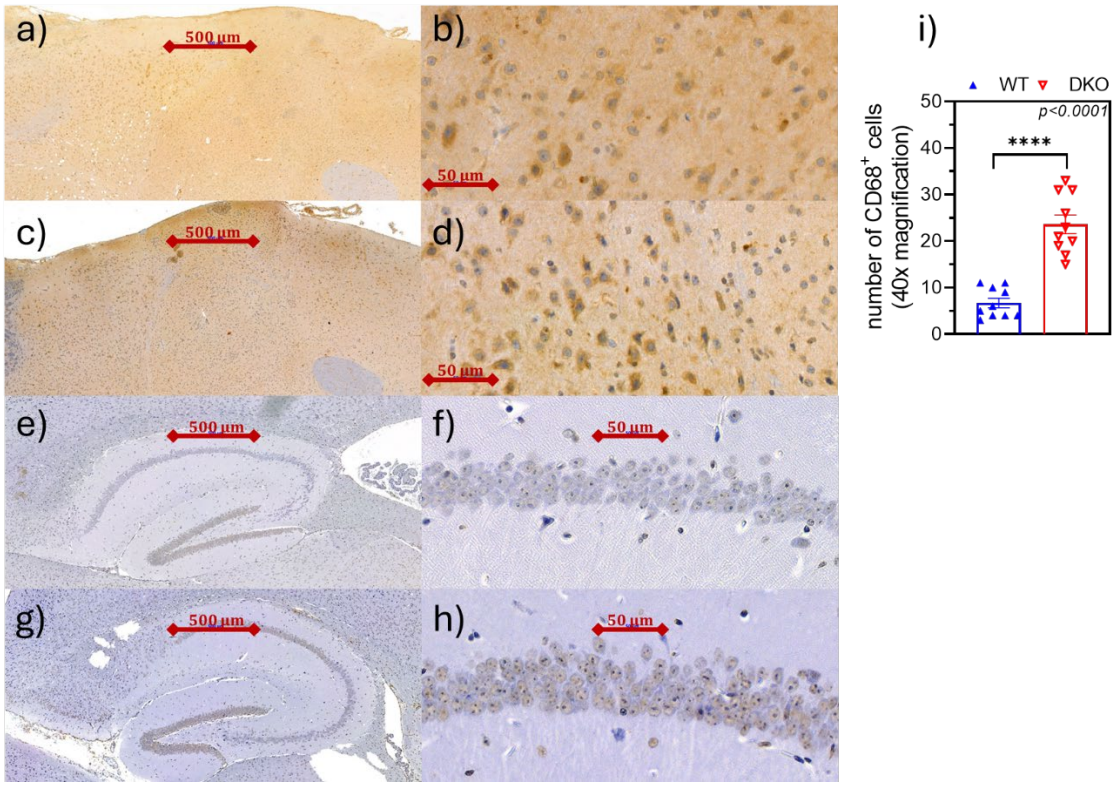

Figure 16. Immunohistology of WT (a, b, e, f) and DKO (c, d, g, h) brains with CD68$^+$ staining (a-d) and with the TUNEL method (e-f). CD68$^+$ cell count (i) was performed at 40x magnification (b, d) in 10 different fields of view. Data were analysed by unpaired t-test. n = 3-4 animals/group.

Hippocampal neuronal loss and dysregulation of mitochondrial dynamics have been observed in the context of cognitive decline and in select neurodegenerative disorders (136-138). In both neuronal and glial cells of DKO animals, the relative expression of dynamin-related protein 1 (Drp1), a key mediator of mitochondrial fission, was found to be elevated (Fig. 17a, f). Consistent with this, the relative expression of mitofusin 2 (Mfn2), which plays a central role in promoting mitochondrial fusion, was significantly reduced in the DKO mice (Fig. 17b, g). The expression level of mitochondrial transcription factor A (MTFA) remained unchanged in DKO group relative to WT, indicating that the introduced combination of mutations does not alter mitochondrial DNA integrity or replication (Fig. 17e, j) (139).

The peroxisome proliferator-activated receptor gamma coactivator 1-α (PGC-1α, Fig 17d, i), a master regulator of mitochondrial biogenesis, and nuclear factor (erythroid-

derived 2)-like 2 (Nrf2, also designated NFE2L2, Fig 17c, h) were both found to be downregulated in neurons and glial cells of DKO mice relative to WT animals. Importantly, Nrf2 is not only regulated by the well-known Keap1-Nrf2 pathway (140), but Aquilano and colleagues also found that PGC-1α and Nrf2 are part of the same redox-signalling pathway controlled by p53 (141). Consistent with previous reports, the reduction in PGC-1α expression in the context of mitochondrial dysfunction has been associated with inflammatory responses, neurite degeneration, and cell death (142-145).

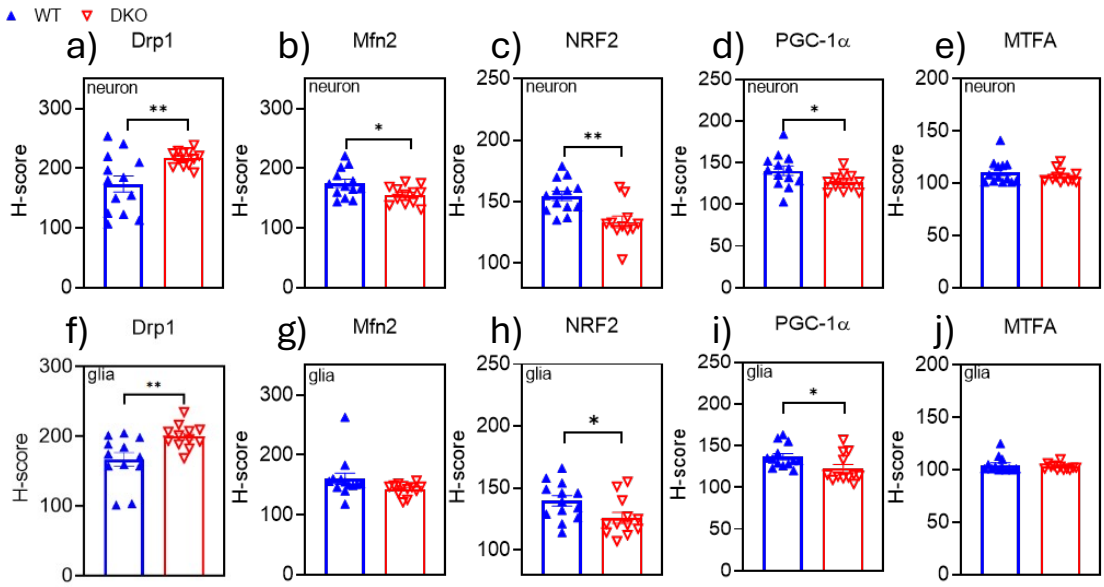

Fig 17. Expression levels of different mitochondria-related signalling molecules in neurons (a-e) and in glial cells (f-j). The H-score reflects the relative expression level of the given antibody inside the cells. Data were analysed by unpaired t-test. n = 11–12/group.

Glucose uptake capacity analysis in the brains using PET-CT imaging

In the context of positron emission tomography (PET) imaging analysis, standardized uptake values (SUV) of [^{18}F]-fluorodeoxyglucose (FDG) were evaluated to assess regional glucose metabolism in WT and DKO mice (146, 147). Given that glucose represents the primary metabolic substrate of the brain, its catabolic rate can be correlated with neuronal function, neuroinflammation and synaptic density. Following image acquisition, regions of interest (ROIs) were delineated for the brain and heart based on corresponding computed tomography (CT) scans. FDG uptake, as reflected by SUV measurements, was elevated in both the brain (Fig. 18c) and heart (Fig. 18f) of DKO

animals relative to controls, with the difference approaching but not reaching statistical significance.

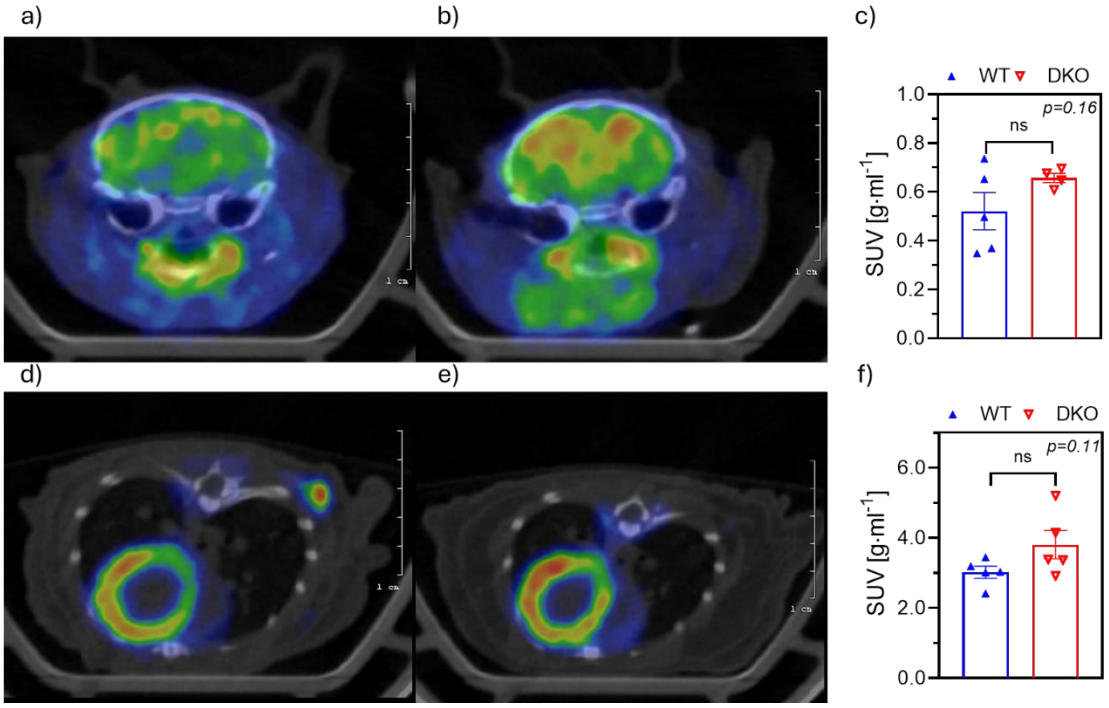

Figure 18. [^{18}F]-fluorodeoxyglucose uptake assessed by PET-CT analysis in WT brain (a), DKO brain (b), WT heart (d) and DKO heart (e). Calculated glucose uptake can be seen in different genotypes in brain (c) and in heart (f). Data were analysed by unpaired t-test. n = 4-5/group.

V. Discussion:

In our experiments, we have studied the effect of combined heterozygous KO of the KGDHc subunits *DLST* and *DLD* on mitochondrial function, animal behaviour, metabolism, and cognitive functions. Importantly, the results on mitochondrial functions are in line with our earlier studies (120) on single heterozygous knock-out models and with those of other studies (33, 57, 126, 127). Furthermore, the largest reduction was observed in the protein expression of E2 and E3 subunits, which was more than 50 % relative to WT. Consistent with the findings previously reported by Kiss (33), both ADP-stimulated O_2 flux and ATP production were significantly diminished in DKO mitochondria energized with α-KG, whereas no such effects were observed when Succ served as the respiratory substrate.This is because Succ enters the TCAc after the reaction catalysed by KGDHc, so Succ-initiated O_2 consumption is not affected by the heterozygous knockout of the KGDHc. Findings in ATP formation indicated that the TCA cycle retained partial functionality in DKO mitochondria, remaining capable of generating succinyl-CoA – albeit in markedly reduced quantities – to sustain matrix SLP. The impaired overall KGDHc activity consequently diminished succinyl-CoA availability for matrix-level SLP in DKO mice relative to controls, resulting in a further decline in mitochondrial ATP content. This reduction in mitochondrial ATP concentration was expected to have contributed to a decrease in $\Delta\Psi_m$, which may in turn have promoted reversal of the adenine nucleotide translocase and the consequent utilization of extramitochondrial ATP to maintain $\Delta\Psi_m$ (32, 33). Such perturbations in mitochondrial ATP homeostasis may render DKO animals particularly susceptible to mitochondrial injury and the deleterious effects of various mitochondrial toxins (126, 127). Compared with single-KO animals (33, 120), the reduction in O_2 flux was greater (close to 50 %) in the DKO mice. Notably, ATP production was already reduced by 50% in single knockout mutants, a magnitude comparable to that observed in DKO mitochondria (33, 148).

Findings on ROS production are in accord with previous studies which were carried out with single *DLST* or *DLD* KO brains (57, 120). Our results further indicate that KGDHc can generate a significant amount of ROS under circumstances when NADH/NAD^+ ratio is high, such as during RET or CI inhibition by rot. The RET is highly susceptible to alterations in $\Delta\Psi_m$ (149) and since ADP induced membrane-depolarization,

a decline in the RET-initiated H_2O_2 formation could be observed (Fig 10). CAT, on the contrary, hyperpolarized the mitochondrial inner membrane, which favoured RET, and hence the H_2O_2 formation was enhanced. In accordance with our previous reports (56, 120) and corroborating evidence from independent studies (57, 64), the predominant source of ROS under conditions of elevated $NADH/NAD^+$ ratio is the E3 subunit of the KGDHc. It follows that heterozygous KO of E2k does not further decrease ROS generation beyond that attributable to E3-mediated mechanisms (119). It is important to note that, while attenuation of ROS generation is generally considered beneficial, it may simultaneously disrupt physiologically relevant ROS-mediated signalling cascades (34). Notably, transient reductions in KGDHc activity may elicit protective cellular responses, such as protein glutathionylation, whereas sustained KGDHc inhibition has been associated with progressive oxidative stress, disruption of calcium homeostasis, and ultimately cell death, as evidenced by studies (150). Moreover, Calingasan et al. published elevated lipid peroxidation in the subgranular zone of *gyrus dentatus* in $DLST^{+/-}$ KO mice (151). Similarly, in $DLD^{+/-}$ KO animals, increased lipid peroxidation in the striatum resulting in cognitive deficit and decreased neurogenesis was reported (126). Discrepancies between direct ROS measurements and indirect oxidative stress markers such as lipid peroxidation reflects the distinct nature of the information each approach provides: direct measurements capture instantaneous ROS production rates, whereas lipid peroxidation reflect cumulative, spatially localized oxidative damage accrued over time. Accordingly, the concurrent application of multiple complementary methodologies is warranted, as substantial tissue-specific oxidative injury may be present even when globally assessed ROS production in isolated mitochondria appears modest.

Interestingly, there were no changes in TCAc related anaplerotic or cataplerotic reactions. Furthermore, *in vivo* metabolic parameters did not change under most of the examined conditions. The absence of changes in amino acid and fatty acid metabolism suggests that under resting conditions, the system has large reserve capacity, hence crucial metabolic intermediates do not accumulate. In particular, the branched-chain amino acids (valine, isoleucine, and leucine), which rely on the branched-chain α-keto acid dehydrogenase complex for their oxidative decarboxylation, as well as glycine – the substrate of the E3-containing glycine cleavage system – and lysine and tryptophan, whose oxidative degradation requires the ketoadipate dehydrogenase complex, did not

differ significantly between DKO and WT groups. Moreover, the mitochondrial ß-oxidation pathway was unaffected and the fatty acid transport into mitochondria (*via* acylcarnitines) was not disturbed.

Taken together, the running performance data (Fig 13), middle-aged DKO mice have a reduced capacity to metabolically compensate for KGDHc deficiency compared to their younger counterparts in the exhaustion test. This difference is even higher in their active (nocturnal) period, which is a logical consequence of higher energy expenditure. Of note, metabolic alterations were not accompanied by fibrotic alterations, which would indicate irreversible progressive pathology, leading to massive cell death in skeletal muscle tissue. Altogether, echocardiographic findings (Fig 14) suggest that DKO mice exhibit mildly compromised resting cardiac function, which is likely to be further exacerbated during physical exertion, thereby providing a mechanistic basis for the reduced endurance capacity observed in the treadmill test. These findings collectively suggest that the observed decline in exercise performance is attributable to a combination of metabolic alterations and deteriorating cardiac function. Based on these results, it is proposed that DKO mice exhibit a reduced compensatory capacity under stress conditions, such as forced physical activity.

Data from cognitive tests (Fig 15) suggest that the reduction in both horizontal and vertical locomotor activity is a consequence of impaired motor function and compromised neuromuscular coordination in DKO mice. It is even possible that long-term KGDHc dysfunction led to psychomotor dysfunction, which was also reported in E3-deficient patients in Ashkenazi Jewish families (78). Consistent with this interpretation, DKO mice required significantly longer latencies to locate the platform in the Morris water maze, further corroborating the presence of motor deficits. Importantly, since the basal activity of age-matched DKO and WT animals did not differ in the metabolic cage, basic motor performance does not appear to be altered in genetically modified animals (data not shown). Taken together, these findings point to a mild but distinguishable cognitive decline in middle-aged DKO animals. This observation is supported by prior studies demonstrating reduced KGDHc activity in post-mortem brain tissue of Alzheimer's disease patients, a finding that correlates with the severity of dementia (152). Furthermore, diminished KGDHc activity has been implicated in memory impairment and deficient neurogenesis in animal models (127, 151, 152).

Our study (119) was the first to report microgliosis in KGDHc KO animals, underscoring the consequences of cumulative genetic alterations. An earlier study highlighted that brain samples from *DLST*$^{+/-}$ or *DLD*$^{+/-}$ mice displayed signs of disturbed neurogenesis, but no further abnormalities (151). Nevertheless, TUNEL staining of the hippocampus formation supported the results of the *in vivo* cognitive test. The CA1 subfield functions as a higher-order comparator within the hippocampal circuit, receiving afferent input from both the CA3 region and the entorhinal cortex (153, 154). Malfunctions in this area could result in behavioural alterations in the animals. Additionally, multiple earlier studies have demonstrated that even mild cognitive impairment can be accompanied by significant CA1 atrophy (155, 156). Notably, DKO mice displayed prominent signs of neurological dysfunction in the absence of any neurotoxin administration or exogenous H_2O_2 treatment, in contrast to what was previously reported in single heterozygous *DLST*$^{+/-}$ mice, where such interventions were required to elicit comparable effects (127, 157).

Our observations (119) are consistent with prior studies reporting upregulated Drp1 expression and diminished Mfn2 levels in the cortices of Alzheimer's disease patients, as well as in SH-SY5Y neuronal cells exhibiting reduced KGDHc activity (137, 138). Frank et al. demonstrated that even mild stress is sufficient to trigger elevated Drp1 levels (158). To sustain this adaptive state, Mfn2 expression must be downregulated, thereby enabling adequately functioning mitochondria to compensate for the heterozygous mutation affecting a key enzymatic component of the TCA cycle (Fig 17). We propose that "underperforming" mitochondria are selectively eliminated via autophagolysosomal degradation, while "overperforming" mitochondria remain structurally intact and functionally active to offset the consequences of the heterozygous genetic modification. This selective mechanism may account for the absence of a proportional reduction in the metabolic parameters observed in our *in vivo* measurements. The present findings further suggest that this compensatory mechanism remains effective only transiently and under conditions of mild stress, as reported by others (159). In the context of double heterozygous KO of *DLST* and *DLD* genes, however, the sustained energetic deficit may impose a mild but chronic stress, ultimately manifesting as cognitive impairment. Notably, such symptoms were not detectable in single KO animals (in the absence of neurotoxic treatment) (127), as the threshold for pathological manifestations is higher in the latter

rodents. An equilibrium between mitochondrial fusion and fission is unavoidable for nonproliferating neurons; otherwise disruption of this balance would lead to severe neurological pathologies such as Charcot Marie Tooth disease type 2A (160). These findings are further strengthened by Toyoma et al., who demonstrated that enhanced AMPK signalling, arising as a consequence of diminished ATP production by oxidative phosphorylation (Fig. 9), promotes mitochondrial fission through increased Drp1 recruitment (Fig. 17a, f) to the mitochondrial membrane via phosphorylation of mitochondrial fission factor (161). Nonetheless, a recent phosphoproteomic study identified an additional AMPK-activated mitochondrial fission protein, called ARMC10, highlighting the central role of cellular energy insufficiency in mitochondrial fragmentation (162). Taken together, these findings suggest that mitochondrial dynamics, indirectly regulated by KGDHc activity, may constitute a critical factor in the progression of neurodegeneration (34).

Importantly, studies in DKO mice indicate an association between KGDHc and the p53-PGC-1α-Nrf2-SOD2 redox axis (Fig 19) (34, 119). A reduced rate of H_2O_2 production was measured in mitochondria isolated from DKO mouse brain across multiple respiratory substrate conditions (Fig. 10), while immunohistochemical analysis revealed downregulation of both Nrf2 and PGC-1α (Fig. 17). These findings collectively highlight the regulatory significance of KGDHc-mediated ROS signalling in the maintenance of mitochondrial physiology. In accordance with that, others have reported impairments in memory and learning in Nrf2-deficient mice (163). Prior studies have reported a reduction in PGC-1α expression in the early stages of Alzheimer's disease, suggesting that KGDHc dysfunction may play a crucial role in the progression of selected neurodegenerative conditions (164). Based on the present data, KGDHc modulates PGC-1α-associated signalling pathways, such that enzymatic downregulation exerts a detrimental effect on mitochondrial biogenesis and stress response mechanisms, including Nrf2. It is further acknowledged that Nrf2 can also be activated by oxidative stress (165, 166). Therefore, the measured Nrf2 concentration reflects the combined influence of KGDHc dysfunction and mild stress (as indicated by Drp1 elevation in Fig. 17). Nevertheless, in DKO mice, the reduction in Nrf2 expression appears to be predominantly attributable to the downstream consequences of KGDHc downregulation, with the contribution of oxidative stress remaining negligible.

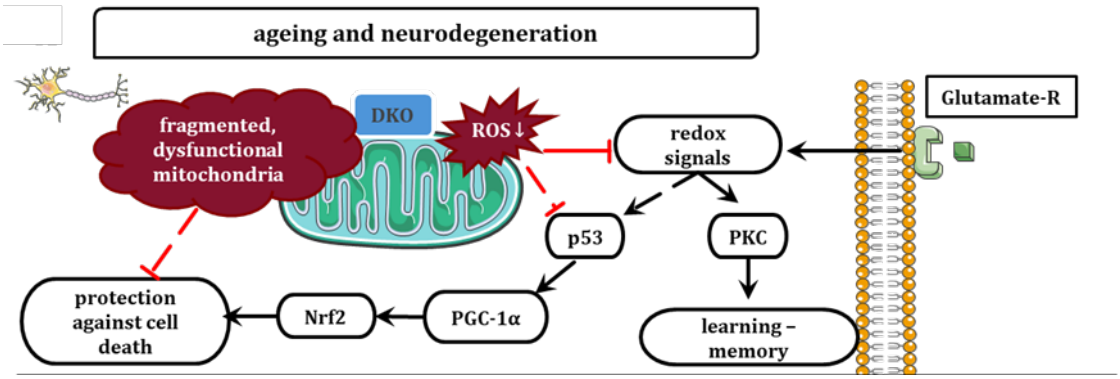

Figure 19. Changes in cellular signalling caused by genetic modification in DKO animals and its effect on ageing and neurodegeneration. Source: Kokas, M., Ambrus, A., Tretter, L. & Komlódi, T. (2026). Interplay between Neuronal Metabolism and Signaling in Model Systems with Impaired α-Ketoglutarate Dehydrogenase Complex Activity. *Biochemistry (Moscow)*, *91* (6), s. 893–909. doi:10.1134/s0006297926600663. (34).

The PET-CT findings raise the question of what underlies the elevated glucose utilization observed in organs experiencing energetic deficits as a consequence of KGDHc dysfunction. One theoretical explanation is that glucose hypermetabolism represents a compensatory metabolic response in DKO brain cells, predominantly neurons, and cardiomyocytes, serving to offset the reduced efficiency of the TCAc and insufficient OXPHOS. Alternatively, as illustrated in Figure 16, neuronal dysfunction was accompanied by the accumulation of inflammatory cells, particularly microglia, which are known to express glucose transporters and may therefore contribute substantially to the observed trend toward increased glucose uptake and the overall perturbation of cerebral metabolism (167, 168). Taken together, these findings are consistent with the mild cognitive decline and the deterioration of cardiac function documented in DKO mice.

VI. Conclusions:

KGDHc functions as a central metabolic regulator that not only catalyses the oxidative decarboxylation of its substrates but also serves as a precise sensor of the cellular redox state and bioenergetic status.

Our study with DKO animals shows that significant substrate-specific alterations in mitochondrial bioenergetics *in vitro* led to only minor metabolic and behavioural differences between the two genotypes *in vivo* under physiological resting condition. This result is accompanied by little or no compensatory response at the transcriptional level of TCAc-related enzymes. The major finding of our study is that the middle-aged transgenic mice performed significantly more poorly than the corresponding younger animals under high energy demand situations, such as under stress. Under these circumstances, the functional alleles of the *DLST* and *DLD* genes were unable to compensate the altered ATP usage. In the fatigue-endurance treadmill test, DKO animals reached exhaustion significantly earlier and covered a considerably shorter total running distance compared to their age-matched controls. This impairment is attributable not only to the underlying energetic deficit, but also to the mildly reduced resting cardiac function, which was further exacerbated upon physical exertion. Furthermore, heterozygous knockout of both DLST and DLD was found to induce microgliosis in the cerebral cortex, neuronal death in the hippocampus, and dysregulation of mitochondrial dynamics and biogenesis. Collectively, these findings indicate significant neuronal involvement and are consistent with a mild but discernible cognitive decline, which was further corroborated, at least in part, by the results of the behavioural test. Only limited differences between younger and older animals were observed in the *in vitro* results (most prominently in ROS production). Naturally, in body composition and in endurance test results middle-aged animals show some differences compared with younger counterparts. In summary we can conclude that age influenced the examined parameters similarly in WT and DKO groups. The limitation of our study is the absence of experiments with elderly rodents (more than 400 days old), which may express a stronger phenotype, but the natural mortality rate would be higher, therefore the number of confounding factors would increase as well.

VII. Summary:

In this work, we have examined *DLST*$^{+/-}$-*DLD*$^{+/-}$ double heterozygous KO mice under *in vitro* and *in vivo* conditions. KGDHc is commonly known as a key enzyme of the TCAc and therefore of mitochondrial energy production. On one hand, the enzyme complex produces NADH for OXPHOS and succinyl-CoA for SLP. On the other hand, it generates a significant amount of ROS under a high NADH/NAD$^+$ ratio. The malfunction of KGDHc is related to many neurodegenerative diseases, such as Alzheimer's disease, Parkinson's disease and Huntington's disease.

Earlier models with genetic modification of the E1k, E2k, or E3 subunit could not identify any alteration in the phenotype, unless an additional toxin or inhibitor was administered. In this study, we aimed to examine the effect of double heterozygous KO of *DLST* and *DLD*. Of note, this genetic modification had previously been generated by another laboratory, however, have published only *in vitro* mitochondrial results.

Our *in vitro* experiments showed that both the O_2 consumption and the ATP synthesis rate were decreased in DKO animals compared to WT in a substrate-specific manner. However, ROS production was also decreased in the mutant groups at a high NADH/NAD$^+$ ratio. In line with that, higher aconitase activity was detected in mutants after incubation with a high concentration of Succ. In the *in vivo* experiments, there were no significant alterations were detected in activity, food and oxygen consumption, or blood amino acid and acylcarnitine profiles. Nevertheless, DKO mice showed decreased performance in the treadmill fatigue-endurance test compared to controls and the cognitive performance of older DKO rodents was reduced. Immunohistology experiments revealed that cortices of older DKO mice suffer from microgliosis and neuronal death was observed in the CA1 subfield of the hippocampus. Additional immunostaining showed that DKO brain mitochondria are fragmented and express lower levels of PGC-1α and Nrf2.

In conclusion, we can state that under resting, physiological circumstances, DKO mice can compensate well. Nonetheless, under high energy demand conditions, DKO mice cannot adequately compensate for the reduced expression of this crucial mitochondrial enzyme.

VIII. References:

1. Lane N. Power, sex, suicide: Mitochondria and the meaning of life: Oxford University Press; 2005.
2. Sagan L. On the origin of mitosing cells. J Theor Biol. 1967;14(3):255-74.
3. Ernster L, Schatz G. Mitochondria: a historical review. J Cell Biol. 1981;91(3 Pt 2):227s-55s.
4. Altmann R. Die Elementarorganismen und ihre Beziehungen zu den Zellen. Leipzig1890.
5. Benda C. Ueber die Spermatogenese der Vertebraten und höherer Evertebraten, II. Theil: Die Histiogenese der Spermien. Archiv für Physiologie. 1898:393-8.
6. Lazarow A, Cooperstein SJ. Studies on the enzymatic basis for the Janus green B staining reaction. J Histochem Cytochem. 1953;1(4):234-41.
7. Anderson S, Bankier AT, Barrell BG, de Bruijn MH, Coulson AR, Drouin J, et al. Sequence and organization of the human mitochondrial genome. Nature. 1981;290(5806):457-65.
8. Lehninger AL. Mitochondria and calcium ion transport. Biochem J. 1970;119(2):129-38.
9. Duchen MR. Mitochondria and calcium: from cell signalling to cell death. J Physiol. 2000;529 Pt 1(Pt 1):57-68.
10. Nicholls DG. Mitochondria and calcium signaling. Cell Calcium. 2005;38(3-4):311-7.
11. Chinopoulos C, Adam-Vizi V. Calcium, mitochondria and oxidative stress in neuronal pathology. Novel aspects of an enduring theme. FEBS J. 2006;273(3):433-50.
12. Cartes-Saavedra B, Ghosh A, Hajnoczky G. The roles of mitochondria in global and local intracellular calcium signalling. Nat Rev Mol Cell Biol. 2025;26(6):456-75.
13. Green DR, Reed JC. Mitochondria and apoptosis. Science. 1998;281(5381):1309-12.
14. Harrington JS, Ryter SW, Plataki M, Price DR, Choi AMK. Mitochondria in health, disease, and aging. Physiol Rev. 2023;103(4):2349-422.
15. Andreyev AY, Kushnareva YE, Starkov AA. Mitochondrial metabolism of reactive oxygen species. Biochemistry (Mosc). 2005;70(2):200-14.

16. Murphy MP. How mitochondria produce reactive oxygen species. Biochem J. 2009;417(1):1-13.
17. Andreyev AY, Kushnareva YE, Murphy AN, Starkov AA. Mitochondrial ROS Metabolism: 10 Years Later. Biochemistry (Mosc). 2015;80(5):517-31.
18. Bernardi P, Vassanelli S, Veronese P, Colonna R, Szabo I, Zoratti M. Modulation of the mitochondrial permeability transition pore. Effect of protons and divalent cations. J Biol Chem. 1992;267(5):2934-9.
19. Starkov AA, Chinopoulos C, Fiskum G. Mitochondrial calcium and oxidative stress as mediators of ischemic brain injury. Cell Calcium. 2004;36(3-4):257-64.
20. Llopis J, McCaffery JM, Miyawaki A, Farquhar MG, Tsien RY. Measurement of cytosolic, mitochondrial, and Golgi pH in single living cells with green fluorescent proteins. Proc Natl Acad Sci U S A. 1998;95(12):6803-8.
21. Mitchell P. Coupling of phosphorylation to electron and hydrogen transfer by a chemi-osmotic type of mechanism. Nature. 1961;191:144-8.
22. Mitchell P, Moyle J. Chemiosmotic hypothesis of oxidative phosphorylation. Nature. 1967;213(5072):137-9.
23. Bing RJ, Siegel A, Ungar I, Gilbert M. Metabolism of the human heart. II. Studies on fat, ketone and amino acid metabolism. Am J Med. 1954;16(4):504-15.
24. Hiltunen JK, Davis EJ. The disposition of citric acid cycle intermediates by isolated rat heart mitochondria. Biochim Biophys Acta. 1981;678(1):115-21.
25. Peuhkurinen KJ, Nuutinen EM, Pietilainen EP, Hiltunen JK, Hassinen IE. Role of pyruvate carboxylation in the energy-linked regulation of pool sizes of tricarboxylic acid-cycle intermediates in the myocardium. Biochem J. 1982;208(3):577-81.
26. Smith CM, Bryla J, Williamson JR. Regulation of mitochondrial alpha-ketoglutarate metabolism by product inhibition at alpha-ketoglutarate dehydrogenase. J Biol Chem. 1974;249(5):1497-505.
27. Koike K, Hamada M, Tanaka N, Otsuka KI, Ogasahara K, Koike M. Properties and subunit composition of the pig heart 2-oxoglutarate dehydrogenase. J Biol Chem. 1974;249(12):3836-42.
28. Koike M, Koike K. Structure, assembly and function of mammalian alpha-keto acid dehydrogenase complexes. Adv Biophys. 1976:187-227.

29. Sheu KF, Blass JP. The alpha-ketoglutarate dehydrogenase complex. Ann N Y Acad Sci. 1999;893:61-78.
30. Szabo E, Nagy B, Czajlik A, Komlodi T, Ozohanics O, Tretter L, et al. Mitochondrial Alpha-Keto Acid Dehydrogenase Complexes: Recent Developments on Structure and Function in Health and Disease. Subcell Biochem. 2024;104:295-381.
31. Hansen GE, Gibson GE. The alpha-Ketoglutarate Dehydrogenase Complex as a Hub of Plasticity in Neurodegeneration and Regeneration. Int J Mol Sci. 2022;23(20).
32. Chinopoulos C. The "B space" of mitochondrial phosphorylation. J Neurosci Res. 2011;89(12):1897-904.
33. Kiss G, Konrad C, Doczi J, Starkov AA, Kawamata H, Manfredi G, et al. The negative impact of alpha-ketoglutarate dehydrogenase complex deficiency on matrix substrate-level phosphorylation. FASEB J. 2013;27(6):2392-406.
34. Kokas M, Ambrus A, Tretter L, Komlódi T. Interplay between Neuronal Metabolism and Signaling in Model Systems with Impaired α-Ketoglutarate Dehydrogenase Complex Activity. Biochemistry (Moscow). 2026;91(6):893-909.
35. Tretter L, Adam-Vizi V. Alpha-ketoglutarate dehydrogenase: a target and generator of oxidative stress. Philos Trans R Soc Lond B Biol Sci. 2005;360(1464):2335-45.
36. Cadenas E, Sies H. Oxidative stress: excited oxygen species and enzyme activity. Adv Enzyme Regul. 1985;23:217-37.
37. Sies H. Oxidative eustress: On constant alert for redox homeostasis. Redox Biol. 2021;41:101867.
38. Selye H. Confusion and controversy in the stress field. J Human Stress. 1975;1(2):37-44.
39. Sies H, Jones DP. Reactive oxygen species (ROS) as pleiotropic physiological signalling agents. Nat Rev Mol Cell Biol. 2020;21(7):363-83.
40. Turrens JF. Mitochondrial formation of reactive oxygen species. J Physiol. 2003;552(Pt 2):335-44.
41. Loew O. A New Enzyme of General Occurrence in Organismis. Science. 1900;11(279):701-2.
42. Fenton HJH. LXXIII.—Oxidation of tartaric acid in presence of iron. J Chem Soc, Trans. 1894;65(0):899-910.

43. Zhang J, Graham DG, Montine TJ, Ho YS. Enhanced N-methyl-4-phenyl-1,2,3,6-tetrahydropyridine toxicity in mice deficient in CuZn-superoxide dismutase or glutathione peroxidase. J Neuropathol Exp Neurol. 2000;59(1):53-61.
44. Aikens J, Dix TA. Perhydroxyl radical (HOO.) initiated lipid peroxidation. The role of fatty acid hydroperoxides. J Biol Chem. 1991;266(23):15091-8.
45. Jomova K, Alomar SY, Alwasel SH, Nepovimova E, Kuca K, Valko M. Several lines of antioxidant defense against oxidative stress: antioxidant enzymes, nanomaterials with multiple enzyme-mimicking activities, and low-molecular-weight antioxidants. Arch Toxicol. 2024;98(5):1323-67.
46. Nagy P, Doka E, Doman A, Paul BD, Balla J, Murphy MP, et al. Multifaceted roles for persulfide species in redox chemical biology. Nat Chem Biol. 2026.
47. Brand MD. Mitochondrial generation of superoxide and hydrogen peroxide as the source of mitochondrial redox signaling. Free Radic Biol Med. 2016;100:14-31.
48. Sies H, Belousov VV, Chandel NS, Davies MJ, Jones DP, Mann GE, et al. Defining roles of specific reactive oxygen species (ROS) in cell biology and physiology. Nat Rev Mol Cell Biol. 2022;23(7):499-515.
49. Gorlach A, Dimova EY, Petry A, Martinez-Ruiz A, Hernansanz-Agustin P, Rolo AP, et al. Reactive oxygen species, nutrition, hypoxia and diseases: Problems solved? Redox Biol. 2015;6:372-85.
50. Jensen PK. Antimycin-insensitive oxidation of succinate and reduced nicotinamide-adenine dinucleotide in electron-transport particles. I. pH dependency and hydrogen peroxide formation. Biochim Biophys Acta. 1966;122(2):157-66.
51. Panov A, Dikalov S, Shalbuyeva N, Taylor G, Sherer T, Greenamyre JT. Rotenone model of Parkinson disease: multiple brain mitochondria dysfunctions after short term systemic rotenone intoxication. J Biol Chem. 2005;280(51):42026-35.
52. Kwong LK, Sohal RS. Substrate and site specificity of hydrogen peroxide generation in mouse mitochondria. Arch Biochem Biophys. 1998;350(1):118-26.
53. Starkov AA, Fiskum G. Regulation of brain mitochondrial H2O2 production by membrane potential and NAD(P)H redox state. J Neurochem. 2003;86(5):1101-7.
54. Tretter L, Takacs K, Hegedus V, Adam-Vizi V. Characteristics of alpha-glycerophosphate-evoked H2O2 generation in brain mitochondria. J Neurochem. 2007;100(3):650-63.

55. Chance B, Williams GR. The respiratory chain and oxidative phosphorylation. Adv Enzymol Relat Subj Biochem. 1956;17:65-134.
56. Tretter L, Adam-Vizi V. Generation of reactive oxygen species in the reaction catalyzed by alpha-ketoglutarate dehydrogenase. J Neurosci. 2004;24(36):7771-8.
57. Starkov AA, Fiskum G, Chinopoulos C, Lorenzo BJ, Browne SE, Patel MS, et al. Mitochondrial alpha-ketoglutarate dehydrogenase complex generates reactive oxygen species. J Neurosci. 2004;24(36):7779-88.
58. Grivennikova VG, Vinogradov AD. Partitioning of superoxide and hydrogen peroxide production by mitochondrial respiratory complex I. Biochim Biophys Acta. 2013;1827(3):446-54.
59. Votyakova TV, Reynolds IJ. DeltaPsi(m)-Dependent and -independent production of reactive oxygen species by rat brain mitochondria. J Neurochem. 2001;79(2):266-77.
60. Komlodi T, Geibl FF, Sassani M, Ambrus A, Tretter L. Membrane potential and delta pH dependency of reverse electron transport-associated hydrogen peroxide production in brain and heart mitochondria. J Bioenerg Biomembr. 2018;50(5):355-65.
61. Chouchani ET, Pell VR, Gaude E, Aksentijevic D, Sundier SY, Robb EL, et al. Ischaemic accumulation of succinate controls reperfusion injury through mitochondrial ROS. Nature. 2014;515(7527):431-5.
62. Yellon DM, Hausenloy DJ. Myocardial reperfusion injury. N Engl J Med. 2007;357(11):1121-35.
63. Quinlan CL, Goncalves RL, Hey-Mogensen M, Yadava N, Bunik VI, Brand MD. The 2-oxoacid dehydrogenase complexes in mitochondria can produce superoxide/hydrogen peroxide at much higher rates than complex I. J Biol Chem. 2014;289(12):8312-25.
64. Bunik VI, Sievers C. Inactivation of the 2-oxo acid dehydrogenase complexes upon generation of intrinsic radical species. Eur J Biochem. 2002;269(20):5004-15.
65. Ambrus A, Nemeria NS, Torocsik B, Tretter L, Nilsson M, Jordan F, et al. Formation of reactive oxygen species by human and bacterial pyruvate and 2-oxoglutarate dehydrogenase multienzyme complexes reconstituted from recombinant components. Free Radic Biol Med. 2015;89:642-50.

66. Ambrus A, Tretter L, Adam-Vizi V. Inhibition of the alpha-ketoglutarate dehydrogenase-mediated reactive oxygen species generation by lipoic acid. J Neurochem. 2009;109 Suppl 1:222-9.
67. Ambrus A, Adam-Vizi V. Molecular dynamics study of the structural basis of dysfunction and the modulation of reactive oxygen species generation by pathogenic mutants of human dihydrolipoamide dehydrogenase. Arch Biochem Biophys. 2013;538(2):145-55.
68. Nemeria NS, Ambrus A, Patel H, Gerfen G, Adam-Vizi V, Tretter L, et al. Human 2-oxoglutarate dehydrogenase complex E1 component forms a thiamin-derived radical by aerobic oxidation of the enamine intermediate. J Biol Chem. 2014;289(43):29859-73.
69. Humphries KM, Szweda LI. Selective inactivation of alpha-ketoglutarate dehydrogenase and pyruvate dehydrogenase: reaction of lipoic acid with 4-hydroxy-2-nonenal. Biochemistry. 1998;37(45):15835-41.
70. McLain AL, Szweda PA, Szweda LI. alpha-Ketoglutarate dehydrogenase: a mitochondrial redox sensor. Free Radic Res. 2011;45(1):29-36.
71. McLain AL, Cormier PJ, Kinter M, Szweda LI. Glutathionylation of alpha-ketoglutarate dehydrogenase: the chemical nature and relative susceptibility of the cofactor lipoic acid to modification. Free Radic Biol Med. 2013;61:161-9.
72. Seim GL, John SV, Arp NL, Fang Z, Pagliarini DJ, Fan J. Nitric oxide-driven modifications of lipoic arm inhibit alpha-ketoacid dehydrogenases. Nat Chem Biol. 2023;19(3):265-74.
73. Csaban D, Pentelenyi K, Toth-Bencsik R, Illes A, Grosz Z, Gezsi A, et al. The Role of the Rare Variants in the Genes Encoding the Alpha-Ketoglutarate Dehydrogenase in Alzheimer's Disease. Life (Basel). 2021;11(4).
74. Yap ZY, Efthymiou S, Seiffert S, Vargas Parra K, Lee S, Nasca A, et al. Bi-allelic variants in OGDHL cause a neurodevelopmental spectrum disease featuring epilepsy, hearing loss, visual impairment, and ataxia. Am J Hum Genet. 2021;108(12):2368-84.
75. Whittle EF, Chilian M, Karimiani EG, Progri H, Buhas D, Kose M, et al. Biallelic variants in OGDH encoding oxoglutarate dehydrogenase lead to a neurodevelopmental disorder characterized by global developmental delay, movement disorder, and metabolic abnormalities. Genet Med. 2023;25(2):100332.

76. Matalon R, Stumpf DA, Michals K, Hart RD, Parks JK, Goodman SI. Lipoamide dehydrogenase deficiency with primary lactic acidosis: favorable response to treatment with oral lipoic acid. J Pediatr. 1984;104(1):65-9.
77. Quinonez SC, Thoene JG. Dihydrolipoamide Dehydrogenase Deficiency. In: Adam MP, Bick S, Mirzaa GM, Pagon RA, Wallace SE, Amemiya A, editors. GeneReviews((R)). Seattle (WA)1993.
78. Shaag A, Saada A, Berger I, Mandel H, Joseph A, Feigenbaum A, et al. Molecular basis of lipoamide dehydrogenase deficiency in Ashkenazi Jews. Am J Med Genet. 1999;82(2):177-82.
79. Shany E, Saada A, Landau D, Shaag A, Hershkovitz E, Elpeleg ON. Lipoamide dehydrogenase deficiency due to a novel mutation in the interface domain. Biochem Biophys Res Commun. 1999;262(1):163-6.
80. Ambrus A, Adam-Vizi V. Human dihydrolipoamide dehydrogenase (E3) deficiency: Novel insights into the structural basis and molecular pathomechanism. Neurochem Int. 2018;117:5-14.
81. Lai JC, Cooper AJ. Brain alpha-ketoglutarate dehydrogenase complex: kinetic properties, regional distribution, and effects of inhibitors. J Neurochem. 1986;47(5):1376-86.
82. Dobolyi A, Bago A, Palkovits M, Nemeria NS, Jordan F, Doczi J, et al. Exclusive neuronal detection of KGDHC-specific subunits in the adult human brain cortex despite pancellular protein lysine succinylation. Brain Struct Funct. 2020;225(2):639-67.
83. Ko LW, Sheu KF, Thaler HT, Markesbery WR, Blass JP. Selective loss of KGDHC-enriched neurons in Alzheimer temporal cortex: does mitochondrial variation contribute to selective vulnerability? J Mol Neurosci. 2001;17(3):361-9.
84. Calingasan NY, Baker H, Sheu KF, Gibson GE. Distribution of the alpha-ketoglutarate dehydrogenase complex in rat brain. J Comp Neurol. 1994;346(3):461-79.
85. Park LC, Calingasan NY, Uchida K, Zhang H, Gibson GE. Metabolic impairment elicits brain cell type-selective changes in oxidative stress and cell death in culture. J Neurochem. 2000;74(1):114-24.
86. Sonnewald U, Schousboe A, Qu H, Waagepetersen HS. Intracellular metabolic compartmentation assessed by 13C magnetic resonance spectroscopy. Neurochem Int. 2004;45(2-3):305-10.

87. Waagepetersen HS, Hansen GH, Fenger K, Lindsay JG, Gibson G, Schousboe A. Cellular mitochondrial heterogeneity in cultured astrocytes as demonstrated by immunogold labeling of alpha-ketoglutarate dehydrogenase. Glia. 2006;53(2):225-31.
88. McKenna MC, Stridh MH, McNair LF, Sonnewald U, Waagepetersen HS, Schousboe A. Glutamate oxidation in astrocytes: Roles of glutamate dehydrogenase and aminotransferases. J Neurosci Res. 2016;94(12):1561-71.
89. Andersen JV, Schousboe A. Milestone Review: Metabolic dynamics of glutamate and GABA mediated neurotransmission - The essential roles of astrocytes. J Neurochem. 2023;166(2):109-37.
90. Salganicoff L, Derobertis E. Subcellular Distribution of the Enzymes of the Glutamic Acid, Glutamine and Gamma-Aminobutyric Acid Cycles in Rat Brain. J Neurochem. 1965;12:287-309.
91. Balazs R, Machiyama Y, Hammond BJ, Julian T, Richter D. The operation of the gamma-aminobutyrate bypath of the tricarboxylic acid cycle in brain tissue in vitro. Biochem J. 1970;116(3):445-61.
92. Hassel B, Bachelard H, Jones P, Fonnum F, Sonnewald U. Trafficking of amino acids between neurons and glia in vivo. Effects of inhibition of glial metabolism by fluoroacetate. J Cereb Blood Flow Metab. 1997;17(11):1230-8.
93. Tretter L, Adam-Vizi V. Inhibition of Krebs cycle enzymes by hydrogen peroxide: A key role of [alpha]-ketoglutarate dehydrogenase in limiting NADH production under oxidative stress. J Neurosci. 2000;20(24):8972-9.
94. Weidinger A, Milivojev N, Hosmann A, Duvigneau JC, Szabo C, Toro G, et al. Oxoglutarate dehydrogenase complex controls glutamate-mediated neuronal death. Redox Biol. 2023;62:102669.
95. Choi DW, Koh JY, Peters S. Pharmacology of glutamate neurotoxicity in cortical cell culture: attenuation by NMDA antagonists. J Neurosci. 1988;8(1):185-96.
96. Truett GE, Heeger P, Mynatt RL, Truett AA, Walker JA, Warman ML. Preparation of PCR-quality mouse genomic DNA with hot sodium hydroxide and tris (HotSHOT). Biotechniques. 2000;29(1):52, 4.
97. Navarro KL, Huss M, Smith JC, Sharp P, Marx JO, Pacharinsak C. Mouse Anesthesia: The Art and Science. ILAR J. 2021;62(1-2):238-73.

98. Chace DH, Kalas TA, Naylor EW. Use of tandem mass spectrometry for multianalyte screening of dried blood specimens from newborns. Clin Chem. 2003;49(11):1797-817.
99. Aranyi T, Tusnady GE. BiSearch: ePCR tool for native or bisulfite-treated genomic template. Methods Mol Biol. 2007;402:385-402.
100. Rosenthal RE, Hamud F, Fiskum G, Varghese PJ, Sharpe S. Cerebral ischemia and reperfusion: prevention of brain mitochondrial injury by lidoflazine. J Cereb Blood Flow Metab. 1987;7(6):752-8.
101. Svab G, Kokas M, Sipos I, Ambrus A, Tretter L. Methylene Blue Bridges the Inhibition and Produces Unusual Respiratory Changes in Complex III-Inhibited Mitochondria. Studies on Rats, Mice and Guinea Pigs. Antioxidants (Basel). 2021;10(2).
102. Fernandez-Vizarra E, Ferrin G, Perez-Martos A, Fernandez-Silva P, Zeviani M, Enriquez JA. Isolation of mitochondria for biogenetical studies: An update. Mitochondrion. 2010;10(3):253-62.
103. Gornall AG, Bardawill CJ, David MM. Determination of serum proteins by means of the biuret reaction. J Biol Chem. 1949;177(2):751-66.
104. Nowotny A. Protein Determination by the Biuret Method. Basic Exercises in Immunochemistry: A Laboratory Manual. 2 ed: Springer Berlin Heidelberg; 1979. p. 168-9.
105. Doerrier C, Garcia-Souza LF, Krumschnabel G, Wohlfarter Y, Meszaros AT, Gnaiger E. High-Resolution FluoRespirometry and OXPHOS Protocols for Human Cells, Permeabilized Fibers from Small Biopsies of Muscle, and Isolated Mitochondria. Methods Mol Biol. 2018;1782:31-70.
106. Williamson JR, Corkey BE. Assay of citric acid cycle intermediates and related compounds--update with tissue metabolite levels and intracellular distribution. Methods Enzymol. 1979;55:200-22.
107. Komlodi T, Tretter L. Methylene blue stimulates substrate-level phosphorylation catalysed by succinyl-CoA ligase in the citric acid cycle. Neuropharmacology. 2017;123:287-98.
108. Tretter L, Ambrus A. Measurement of ROS homeostasis in isolated mitochondria. Methods Enzymol. 2014;547:199-223.

109. Miwa S, Treumann A, Bell A, Vistoli G, Nelson G, Hay S, et al. Carboxylesterase converts Amplex red to resorufin: Implications for mitochondrial H2O2 release assays. Free Radic Biol Med. 2016;90:173-83.
110. Hausladen A, Fridovich I. Measuring nitric oxide and superoxide: rate constants for aconitase reactivity. Methods Enzymol. 1996;269:37-41.
111. Kuti D, Winkler Z, Horvath K, Juhasz B, Szilvasy-Szabo A, Fekete C, et al. The metabolic stress response: Adaptation to acute-, repeated- and chronic challenges in mice. iScience. 2022;25(8):104693.
112. Dougherty JP, Springer DA, Gershengorn MC. The Treadmill Fatigue Test: A Simple, High-throughput Assay of Fatigue-like Behavior for the Mouse. J Vis Exp. 2016(111).
113. Sayour NV, Gergely TG, Varadi B, Toth VE, Agg B, Kovacs T, et al. Comparison of mouse models of heart failure with reduced ejection fraction. ESC Heart Fail. 2025;12(1):87-100.
114. Zacchigna S, Paldino A, Falcao-Pires I, Daskalopoulos EP, Dal Ferro M, Vodret S, et al. Towards standardization of echocardiography for the evaluation of left ventricular function in adult rodents: a position paper of the ESC Working Group on Myocardial Function. Cardiovasc Res. 2021;117(1):43-59.
115. Harkany T, Sasvari M, Nyakas C. Chronic ethanol ingestion-induced changes in open-field behavior and oxidative stress in the rat. Pharmacol Biochem Behav. 1997;58(1):195-201.
116. Ennaceur A, Meliani K. A new one-trial test for neurobiological studies of memory in rats. III. Spatial vs. non-spatial working memory. Behav Brain Res. 1992;51(1):83-92.
117. Nyakas C, Felszeghy K, Szabo R, Keijser JN, Luiten PG, Szombathelyi Z, et al. Neuroprotective effects of vinpocetine and its major metabolite cis-apovincaminic acid on NMDA-induced neurotoxicity in a rat entorhinal cortex lesion model. CNS Neurosci Ther. 2009;15(2):89-99.
118. Morris R. Developments of a water-maze procedure for studying spatial learning in the rat. J Neurosci Methods. 1984;11(1):47-60.
119. Kokas M, Budai A, Kadar A, Mozaffaritabar S, Zhou L, Teglas T, et al. Microgliosis, neuronal death, minor behavioral abnormalities and reduced endurance

performance in alpha-ketoglutarate dehydrogenase complex deficient mice. Redox Biol. 2025;85:103743.

120. Horvath G, Svab G, Komlodi T, Ravasz D, Kacso G, Doczi J, et al. Reverse and Forward Electron Flow-Induced H(2)O(2) Formation Is Decreased in alpha-Ketoglutarate Dehydrogenase (alpha-KGDH) Subunit (E2 or E3) Heterozygote Knock Out Animals. Antioxidants (Basel). 2022;11(8).

121. Wojtczak AB. Inhibitory action of oxaloacetate on succinate oxidation in rat-liver mitochondria and the mechanism of its reversal. Biochim Biophys Acta. 1969;172(1):52-65.

122. Wojtczak L, Wojtczak AB, Ernster L. The inhibition of succinate dehydrogenase by oxalacetate. Biochim Biophys Acta. 1969;191(1):10-21.

123. Zhang J, Wang YT, Miller JH, Day MM, Munger JC, Brookes PS. Accumulation of Succinate in Cardiac Ischemia Primarily Occurs via Canonical Krebs Cycle Activity. Cell Rep. 2018;23(9):2617-28.

124. Turrens JF, Alexandre A, Lehninger AL. Ubisemiquinone is the electron donor for superoxide formation by complex III of heart mitochondria. Arch Biochem Biophys. 1985;237(2):408-14.

125. Rimal S, Tantray I, Li Y, Pal Khaket T, Li Y, Bhurtel S, et al. Reverse electron transfer is activated during aging and contributes to aging and age-related disease. EMBO Rep. 2023;24(4):e55548.

126. Klivenyi P, Starkov AA, Calingasan NY, Gardian G, Browne SE, Yang L, et al. Mice deficient in dihydrolipoamide dehydrogenase show increased vulnerability to MPTP, malonate and 3-nitropropionic acid neurotoxicity. J Neurochem. 2004;88(6):1352-60.

127. Yang L, Shi Q, Ho DJ, Starkov AA, Wille EJ, Xu H, et al. Mice deficient in dihydrolipoyl succinyl transferase show increased vulnerability to mitochondrial toxins. Neurobiol Dis. 2009;36(2):320-30.

128. Holness CL, da Silva RP, Fawcett J, Gordon S, Simmons DL. Macrosialin, a mouse macrophage-restricted glycoprotein, is a member of the lamp/lgp family. J Biol Chem. 1993;268(13):9661-6.

129. Rabinowitz SS, Gordon S. Macrosialin, a macrophage-restricted membrane sialoprotein differentially glycosylated in response to inflammatory stimuli. J Exp Med. 1991;174(4):827-36.
130. Van Muiswinkel FL, Veerhuis R, Eikelenboom P. Amyloid beta protein primes cultured rat microglial cells for an enhanced phorbol 12-myristate 13-acetate-induced respiratory burst activity. J Neurochem. 1996;66(6):2468-76.
131. Kumar A, Barrett JP, Alvarez-Croda DM, Stoica BA, Faden AI, Loane DJ. NOX2 drives M1-like microglial/macrophage activation and neurodegeneration following experimental traumatic brain injury. Brain Behav Immun. 2016;58:291-309.
132. Norrington M, Rathi N, Jenkinson MD, Mills SJ. Neuroinflammation preceding primary central nervous system lymphoma (PCNSL) - Case reports and literature review. J Clin Neurosci. 2021;89:381-8.
133. Tarantini S, Valcarcel-Ares MN, Yabluchanskiy A, Tucsek Z, Hertelendy P, Kiss T, et al. Nrf2 Deficiency Exacerbates Obesity-Induced Oxidative Stress, Neurovascular Dysfunction, Blood-Brain Barrier Disruption, Neuroinflammation, Amyloidogenic Gene Expression, and Cognitive Decline in Mice, Mimicking the Aging Phenotype. J Gerontol A Biol Sci Med Sci. 2018;73(7):853-63.
134. Gavrieli Y, Sherman Y, Ben-Sasson SA. Identification of programmed cell death in situ via specific labeling of nuclear DNA fragmentation. J Cell Biol. 1992;119(3):493-501.
135. Liu X, Wu Z, Hayashi Y, Nakanishi H. Age-dependent neuroinflammatory responses and deficits in long-term potentiation in the hippocampus during systemic inflammation. Neuroscience. 2012;216:133-42.
136. Kim J, Moody JP, Edgerly CK, Bordiuk OL, Cormier K, Smith K, et al. Mitochondrial loss, dysfunction and altered dynamics in Huntington's disease. Hum Mol Genet. 2010;19(20):3919-35.
137. Manczak M, Calkins MJ, Reddy PH. Impaired mitochondrial dynamics and abnormal interaction of amyloid beta with mitochondrial protein Drp1 in neurons from patients with Alzheimer's disease: implications for neuronal damage. Hum Mol Genet. 2011;20(13):2495-509.
138. Banerjee K, Munshi S, Xu H, Frank DE, Chen HL, Chu CT, et al. Mild mitochondrial metabolic deficits by alpha-ketoglutarate dehydrogenase inhibition cause

prominent changes in intracellular autophagic signaling: Potential role in the pathobiology of Alzheimer's disease. Neurochem Int. 2016;96:32-45.
139. Kang D, Kim SH, Hamasaki N. Mitochondrial transcription factor A (TFAM): roles in maintenance of mtDNA and cellular functions. Mitochondrion. 2007;7(1-2):39-44.
140. Suzuki T, Motohashi H, Yamamoto M. Toward clinical application of the Keap1-Nrf2 pathway. Trends Pharmacol Sci. 2013;34(6):340-6.
141. Aquilano K, Baldelli S, Pagliei B, Cannata SM, Rotilio G, Ciriolo MR. p53 orchestrates the PGC-1alpha-mediated antioxidant response upon mild redox and metabolic imbalance. Antioxid Redox Signal. 2013;18(4):386-99.
142. Budai A, Horvath G, Tretter L, Radak Z, Koltai E, Bori Z, et al. Mitochondrial function after associating liver partition and portal vein ligation for staged hepatectomy in an experimental model. Br J Surg. 2019;106(1):120-31.
143. Fard-Aghaie MH, Budai A, Daradics N, Horvath G, Oldhafer KJ, Szijarto A, et al. The effects of physical prehabilitation: Improved liver regeneration and mitochondrial function after ALPPS operation in a rodent model. J Hepatobiliary Pancreat Sci. 2021;28(8):692-702.
144. Daradics N, Horvath G, Tretter L, Paal A, Fulop A, Budai A, et al. The effect of Cyclophilin D depletion on liver regeneration following associating liver partition and portal vein ligation for staged hepatectomy. PLoS One. 2022;17(7):e0271606.
145. You W, Knoops K, Berendschot T, Benedikter BJ, Webers CAB, Reutelingsperger CPM, et al. PGC-1a mediated mitochondrial biogenesis promotes recovery and survival of neuronal cells from cellular degeneration. Cell Death Discov. 2024;10(1):180.
146. Tai YF, Piccini P. Applications of positron emission tomography (PET) in neurology. J Neurol Neurosurg Psychiatry. 2004;75(5):669-76.
147. Szollosi D, Hegedus N, Veres DS, Futo I, Horvath I, Kovacs N, et al. Evaluation of Brain Nuclear Medicine Imaging Tracers in a Murine Model of Sepsis-Associated Encephalopathy. Mol Imaging Biol. 2018;20(6):952-62.
148. Saada A, Aptowitzer I, Link G, Elpeleg ON. ATP synthesis in lipoamide dehydrogenase deficiency. Biochem Biophys Res Commun. 2000;269(2):382-6.

149. Korshunov SS, Skulachev VP, Starkov AA. High protonic potential actuates a mechanism of production of reactive oxygen species in mitochondria. FEBS Lett. 1997;416(1):15-8.
150. Chen H, Denton TT, Xu H, Calingasan N, Beal MF, Gibson GE. Reductions in the mitochondrial enzyme alpha-ketoglutarate dehydrogenase complex in neurodegenerative disease - beneficial or detrimental? J Neurochem. 2016;139(5):823-38.
151. Calingasan NY, Ho DJ, Wille EJ, Campagna MV, Ruan J, Dumont M, et al. Influence of mitochondrial enzyme deficiency on adult neurogenesis in mouse models of neurodegenerative diseases. Neuroscience. 2008;153(4):986-96.
152. Bubber P, Haroutunian V, Fisch G, Blass JP, Gibson GE. Mitochondrial abnormalities in Alzheimer brain: mechanistic implications. Ann Neurol. 2005;57(5):695-703.
153. Chen J, Olsen RK, Preston AR, Glover GH, Wagner AD. Associative retrieval processes in the human medial temporal lobe: hippocampal retrieval success and CA1 mismatch detection. Learn Mem. 2011;18(8):523-8.
154. Geiller T, Royer S, Choi JS. Segregated Cell Populations Enable Distinct Parallel Encoding within the Radial Axis of the CA1 Pyramidal Layer. Exp Neurobiol. 2017;26(1):1-10.
155. Braak H, Braak E. Neuropathological stageing of Alzheimer-related changes. Acta Neuropathol. 1991;82(4):239-59.
156. de Flores R, La Joie R, Chetelat G. Structural imaging of hippocampal subfields in healthy aging and Alzheimer's disease. Neuroscience. 2015;309:29-50.
157. Shi Q, Chen HL, Xu H, Gibson GE. Reduction in the E2k subunit of the alpha-ketoglutarate dehydrogenase complex has effects independent of complex activity. J Biol Chem. 2005;280(12):10888-96.
158. Frank M, Duvezin-Caubet S, Koob S, Occhipinti A, Jagasia R, Petcherski A, et al. Mitophagy is triggered by mild oxidative stress in a mitochondrial fission dependent manner. Biochim Biophys Acta. 2012;1823(12):2297-310.
159. Graf A, Trofimova L, Loshinskaja A, Mkrtchyan G, Strokina A, Lovat M, et al. Up-regulation of 2-oxoglutarate dehydrogenase as a stress response. Int J Biochem Cell Biol. 2013;45(1):175-89.

160. Youle RJ, van der Bliek AM. Mitochondrial fission, fusion, and stress. Science. 2012;337(6098):1062-5.
161. Toyama EQ, Herzig S, Courchet J, Lewis TL, Jr., Loson OC, Hellberg K, et al. Metabolism. AMP-activated protein kinase mediates mitochondrial fission in response to energy stress. Science. 2016;351(6270):275-81.
162. Chen Z, Lei C, Wang C, Li N, Srivastava M, Tang M, et al. Global phosphoproteomic analysis reveals ARMC10 as an AMPK substrate that regulates mitochondrial dynamics. Nat Commun. 2019;10(1):104.
163. Rojo AI, Pajares M, Rada P, Nunez A, Nevado-Holgado AJ, Killik R, et al. NRF2 deficiency replicates transcriptomic changes in Alzheimer's patients and worsens APP and TAU pathology. Redox Biol. 2017;13:444-51.
164. Singulani MP, Pereira CPM, Ferreira AFF, Garcia PC, Ferrari GD, Alberici LC, et al. Impairment of PGC-1alpha-mediated mitochondrial biogenesis precedes mitochondrial dysfunction and Alzheimer's pathology in the 3xTg mouse model of Alzheimer's disease. Exp Gerontol. 2020;133:110882.
165. Baldelli S, Aquilano K, Ciriolo MR. Punctum on two different transcription factors regulated by PGC-1alpha: nuclear factor erythroid-derived 2-like 2 and nuclear respiratory factor 2. Biochim Biophys Acta. 2013;1830(8):4137-46.
166. George M, Reddy AP, Reddy PH, Kshirsagar S. Unraveling the NRF2 confusion: Distinguishing nuclear respiratory factor 2 from nuclear erythroid factor 2. Ageing Res Rev. 2024;98:102353.
167. Backes H, Walberer M, Ladwig A, Rueger MA, Neumaier B, Endepols H, et al. Glucose consumption of inflammatory cells masks metabolic deficits in the brain. Neuroimage. 2016;128:54-62.
168. Xiang X, Wind K, Wiedemann T, Blume T, Shi Y, Briel N, et al. Microglial activation states drive glucose uptake and FDG-PET alterations in neurodegenerative diseases. Sci Transl Med. 2021;13(615):eabe5640.

IX. Bibliography of the candidate's publications:

Thesis related publications:

Kokas, M., Budai, A., Kádár, A., Mozaffaritabar, S., Zhou, L., Téglás, T., Orova, R. S., Gáspár, D., Németh, K., Toth, D. M., Sayour, N. V., Kovácsházi, C., Xue, A., Szatmári, R. Z., Törőcsik, B., Máthé, D., Kovács, N., Szigeti, K., Nagy, P., Szatmári, I., … Ambrus, A. (2025). Microgliosis, neuronal death, minor behavioral abnormalities and reduced endurance performance in alpha-ketoglutarate dehydrogenase complex deficient mice. *Redox biology*, *85*, 103743. https://doi.org/10.1016/j.redox.2025.103743

Kokas, M., Ambrus, A., Tretter, L. & Komlódi, T. (2026). Interplay between Neuronal Metabolism and Signaling in Model Systems with Impaired α-Ketoglutarate Dehydrogenase Complex Activity. *Biochemistry (moscow)*, *91* (6), s. 893–909. https://doi:10.1134/s0006297926600663

Not related to the thesis:

Sváb, G., Kokas, M., Sipos, I., Ambrus, A., & Tretter, L. (2021). Methylene Blue Bridges the Inhibition and Produces Unusual Respiratory Changes in Complex III-Inhibited Mitochondria. Studies on Rats, Mice and Guinea Pigs. *Antioxidants (Basel, Switzerland)*, *10*(2), 305. https://doi.org/10.3390/antiox10020305

X. Acknowledgements:

I would like to thank all the people who supported and helped me, especially my supervisors, Professor (and captain) László Tretter and Tímea Komlódi. Without them, I could not have reached this point in my life, for which I am deeply grateful. I am also thankful to our assistants, Katalin Takács and Andrea Várnagy, and to all our TDK students who helped me with many projects over the years here in the institute. I am grateful to the head of the department, Professor László Csanády, who allowed me to work and teach here. Finally, I would like to thank my family and friends, who supported me no matter what happened in life.

Semmelweis Egyetem
Doktori Iskola

Semmelweis Egyetem
Intézményi azonosító: FI 62576

NYILATKOZAT EREDETISÉGRŐL ÉS SZERZŐI JOGRÓL

a PhD disszertáció elkészítésére vonatkozó szabályok betartásáról

Alulírott Dr. Kokas Márton jelen nyilatkozat aláírásával kijelentem, hogy a 'BIOENERGETIC CONSEQUENCES OF HETEROZYGOUS ALPHA-KETOGLUTARATE DEHYDROGENASE COMPLEX MUTATION' című PhD értekezésem önálló munkám, a dolgozat készítése során betartottam a szerzői jogról szóló 1999. évi LXXVI tv. vonatkozó rendelkezéseit, a már megjelent vagy közlés alatt álló közlemény(ek)ből felhasznált ábra/szöveg nem sérti a kiadó vagy más jogi vagy természetes személy jogait.

Jelen nyilatkozat aláírásával tudomásul veszem, hogy amennyiben igazolható, hogy a dolgozatban nem saját eredményeimet használtam fel vagy a dolgozattal kapcsolatban szerzői jog megsértése merül fel, a Semmelweis Egyetem megtagadja PhD dolgozatom befogadását, velem szemben fegyelmi eljárást indít, illetve visszavonja a már odaítélt PhD fokozatot.

A dolgozat befogadásának megtagadása és a fegyelmi eljárás indítása nem érinti a szerzői jogsértés miatti egyéb (polgári jogi, szabálysértési jogi, büntetőjogi) jogkövetkezményeket.

Tudomásul veszem, hogy a PhD értekezés nyilvánosan elérhető formában feltöltésre kerül az Országos Doktori Tanács honlapjára.

Budapest, 2026. 07. 02.

aláírás